Basic properties of the dimension stone used in the construction of the Zagreb Cathedral

Katalinić, Franjo

Master's thesis / Diplomski rad

2022

Degree Grantor / Ustanova koja je dodijelila akademski / stručni stupanj: **University of Zagreb, Faculty of Mining, Geology and Petroleum Engineering / Sveučilište u Zagrebu, Rudarsko-geološko-naftni fakultet**

Permanent link / Trajna poveznica: https://urn.nsk.hr/urn:nbn:hr:169:560912

Rights / Prava: In copyright / Zaštićeno autorskim pravom.

Download date / Datum preuzimanja: **2025-03-21**

Repository / Repozitorij:

Faculty of Mining, Geology and Petroleum Engineering Repository, University of Zagreb

UNIVERSITY OF ZAGREB
FACULTY OF MINING, GEOLOGY AND PETROLEUM ENGINEERING
Graduate study programme – Mining engineering

BASIC PROPERTIES OF THE DIMENSION STONE USED IN THE CONSTRUCTION OF THE ZAGREB CATHEDRAL

Master thesis

Franjo Katalinić
R4264

Zagreb, 2022

KLASA: 602-01/22-01/153
URBROJ: 251-70-11-22-12
U Zagrebu, 11.07.2022.

Franjo Katalinić, student

RJEŠENJE O ODOBRENJU TEME

Na temelju vašeg zahtjeva primljenog pod KLASOM 602-01/22-01/153, URBROJ: 251-70-11-22-11 od 07.07.2022. priopćujemo vam temu diplomskog rada koja glasi:

BASIC PROPERTIES OF THE DIMENSION STONE USED IN THE CONSTRUCTION OF THE ZAGREB CATHEDRAL

Za voditeljicu ovog diplomskog rada imenuje se u smislu Pravilnika o izradi i obrani diplomskog rada Izv. prof. dr. sc. Ana Maričić nastavnik Rudarsko-geološko-naftnog-fakulteta Sveučilišta u Zagrebu

Voditelj

(potpis)

Izv. prof. dr. sc. Ana Maričić

(titula, ime i prezime)

Predsjednik povjerenstva za završne i diplomske ispite:

(potpis)

Izv.prof.dr.sc. Dubravko Domitrović

(titula, ime i prezime)

Prodekan za nastavu i studente:

(potpis)

Izv.prof.dr.sc. Borivoje Pašić

(titula, ime i prezime)

Sveučilište u Zagrebu
Rudarsko-geološko-naftni fakultet

OSNOVNA SVOJSTVA PRIRODNOG KAMENA KORIŠTENOG U IZGRADNJI ZAGREBAČKE KATEDRALE

Franjo Katalinić

Rad izrađen: Sveučilište u Zagrebu
Rudarsko-geološko-naftni fakultet
Zavod za mineralogiju, petrologiju i mineralne sirovine
Pierottijeva 6, 10 000 Zagreb

Sažetak

U ovom istraživanju ispitivano je 20 uzoraka kamena sa Zagrebačke katedrale. Uzorci su blokova litotamnijskog vapnenca i pješčenjaka koji su pali s katedrale tijekom potresa u Zagrebu 2020. godine. Osnovna svojstva koja su ispitivana su: mineraloški sastav temeljen na rendgenskoj difrakciji, gustoća, prostorna masa, otvorena i ukupna poroznost te apsorpcija vode pri atmosferskom tlaku. Rezultati su pokazali da uzorci litotamnijskog vapnenca i pješčenjaka posjeduju vrijednosti osnovnih svojstava unutar normalnog raspona za pojedinu vrstu stijene.

Ključne riječi: Zagrebačka katedrala, litotamnijski vapnenac, potres u Zagrebu 2020., rendgenska difrakcija, gustoća, prostorna masa, otvorena i ukupna poroznost, upijanje vode pri atmosferskom tlaku

Završni rad sadrži: 68 stranice, 16 tablica, 43 slika, 0 priloga i 34 reference.

Jezik izvornika: Engleski

Pohrana rada: Knjižnica Rudarsko-geološko-naftnog fakulteta, Pierottijeva 6, Zagreb

Mentori: Dr. sc. Ana Maričić, izvanredni profesor RGNF

Pomagao pri izradi/komentor: Dipl. ing. Vinko Baranašić, viši tehničar RGNF
Dipl. ing. Neven Tadej, viši stručni suradnik RGNF

Ocjenjivači: Dr. sc. Ana Maričić, izvanredni profesor RGNF
Dr. sc. Zlatko Briševac, izvanredni profesor RGNF
Dr. sc. Uroš Barudžija, izvanredni profesor RGNF

Datum obrane: 15.7.2022., Rudarsko-geološko-naftni fakultet Sveučilišta u Zagrebu

University of Zagreb
Faculty of Mining, Geology and Petroleum Engineering

Master's Thesis

BASIC PROPERTIES OF THE DIMENSION STONE USED IN THE CONSTRUCTION OF THE ZAGREB CATHEDRAL

Franjo Katalinić

Thesis completed at: University of Zagreb
Faculty of mining, Geology and Petroleum Engineering
Department of mineralogy, petrology and mineral resources
Pierottijeva 6, 10 000 Zagreb

Abstract

In this study, 20 samples from the Zagreb Cathedral were tested. The samples were taken from lithothamnium limestone and sandstone blocks that fell during the 2020 earthquake in Zagreb. The basic properties that were tested were: mineralogical composition based on X-Ray Diffraction, real and apparent density, open and total porosity, and water absorption at atmospheric pressure. The results showed that the lithotanium limestone and sandstone samples had values of aforementioned properties within the normal range for their respective rock type.

Keywords: Zagreb Cathedral, lithothamnium limestone, 2020 earthquake in Zagreb, X-Ray Diffraction, real and apparent density, open and total porosity, water absorption at atmospheric pressure

Thesis contains: 68 pages, 16 tables, 43 figures, 0 appendixes and 34 references.

Original in: English

Archived in: Library of Faculty of Mining, Geology and Petroleum Engineering, Pierottijeva 6, Zagreb

Supervisors: Ana Maričić, PhD

Tech. assistance: Vinko Baranašić, dipl. ing.
Neven Tadej, dipl. ing.

Reviewers: Ana Maričić, PhD
Zlatko Briševac, PhD
Uroš Barudžija, PhD

Defence date: July 15, 2022, Faculty of Mining, Geology and Petroleum Engineering, University of Zagreb

ACKNOWLEDGMENTS

I would like to thank the laboratory technicians Branka Prša and Vinko Baranašić for their help during the preparation and processing of the samples and for guiding me through the laboratory analysis procedures.

I would like to thank Michaela Hruškova Hasan, PhD, for helping me with calcimetry, providing equipment for microphotographing the samples and showing me how to determine the colours of the samples.

I would like to thank Neven Tadej, dipl. ing., for the great amount of time and effort invested in the interpretation of the X-ray diffraction results.

Finally, a big thank you to my supervisor, Ani Maričić, PhD, without whose efforts and leadership this thesis would not exist.

TABLE OF CONTENT

LIST OF FIGURES

LIST OF TABLES

LIST OF SYMBOLS

Symbol	Unit	Description
A_b	%	water absorption at atmospheric pressure
m_1	g	the mass of the test portion of the sample
m_2	g	the mean mass of the calcium carbonate standard
m_d	g	mass of the dry sample
m_e	g	mass of the specimen ground and dried
m_h	g	mass the sample immersed in water
m_s	g	mass of the saturated sample
m_w	g	mass of the water in the pycnometer
p	%	total porosity of the sample
p_o	%	open porosity of the sample
V_b	ml	apparent volume of the sample
V_o	ml	volume of open pores of the sample
V_p	ml	volume of the pycnometer
V_s	ml	volume of liquid displaced by the mass m_e
V_u	ml	volume of the sample
V_w	ml	volume of the water in the pycnometer
ρ_b	kg/m^3	real density of the sample
ρ_r	g	real density of the sample
ρ_{rh}	kg/m^3	density of water

1. INTRODUCTION

Lithothamnium limestone and litavac stone are the most used natural stone varieties in the Zagreb city including in the Zagreb Cathedral since they were exploited nearby, in the Medvednica Mt. The quarries at Gornji Vrape and Bizek supplied the stone varieties (Crnković, 1992, 1996). Famous buildings besides Cathedral include the Croatian National Theatre, parts of Mirogoj Arcades, City Assembly of The City of Zagreb, pedestals at the Banski dvori, the cornice of the Postal building in Jurišićeva street, facades and pillars of the City Café (now known as Johann Franck) and the City Savings Bank on the Ban Josip Jelačić square. Also, facades of numerous Zagreb buildings are made from this variety of limestone (Crnković & Poggi, 1995, Fio Firi & Maričić, 2020).

Today, there are similar terms in the English language that are commonly used for rock with highly decorative features. According to the United States Geological Survey (Dolley, 2018), *dimension stone* is „natural rock material quarried for the purpose of obtaining blocks or slabs that meet specifications as to size (width, length, and thickness) and shape". It is an unspecific rock suitable for construction purposes, as opposed to crushed stone or aggregate. Classical dimension stone is ornamental in use. This type of stone is commonly used in buildings and constructions (e.g., cladding and paving), and in the making of sculptures, monuments, and memorials (e.g., tombstones). The term refers to any stone that can be quarried in large blocks and then processed into smaller, ready-to-sell products such as slabs, blocks, tiles, or flagstones (Epiroc, 2020).

The second term being used is *building stone.* It can be defined as a sound rock used in some situation in the construction as a massive dressed or undressed unit. Sandstones and limestones used in forts, retaining walls and boundary walls and as blocks in stone buildings are typical building stones (Malik, 2018).

The third term is *natural stone.* It refers to a classic, high-quality material historically used in construction (Deutscher Naturwerkstein-Verband e.V., 2016). These stones include diorite, quartzite, marble, travertine, granite, and the like. Natural stones are found in natural mines as opposed to artificially made stone called agglomerated (Deutscher Naturwerkstein-Verband e.V., 2016).

Dimension stone production has increased significantly worldwide over the past 20 years, particularly for construction projects where architects are increasingly utilizing the vast range of colours, textures, and finishes that natural stone can provide. China, India, Turkey, Iran, Italy, Brazil, and Spain make up around two-thirds of the world's dimension stone production now (Epiroc, 2020).

In this thesis, the emphasis was on natural stone samples that were built in the Zagreb Cathedral. During the earthquake that struck Zagreb on March 22, 2020, many large stone blocks fell from the Zagreb Cathedral. Stone samples for determining the mineral composition and basic physical properties were taken from such blocks. Two sets of samples were analysed. The first set of samples were of lithothamnium limestone, and the second set were of sandstone. These basic properties are important in determining the possibility of applying a limestone variety as building material.

X-ray diffraction and calcination was used to determine the mineral composition of the lithothamnium limestone samples. Two norms for determining physical properties on two sets of samples (10 samples per set – lithothamnium samples and sandstone samples) were used. The norm HRN EN 1936 „Natural stone test methods – Determination of real density and apparent density, and of total and open porosity (EN 1936:1999) “ was used for the determination of real density and apparent density, and of total and open porosity, while the norm HRN EN 13755 „Natural stone test methods – Determination of water absorption at atmospheric pressure“ was used to determine the water absorption at atmospheric pressure“.

2. BRIEF HISTORY OF THE ZAGREB CATHEDRAL CONSTRUCTION AND RENOVATION

Zagreb Cathedral was formerly known as St. Stephen's Cathedral. Today, the Cathedral is dedicated to the Assumption of the Blessed Virgin Mary and to kings Saint Stephen and Saint Ladislaus (Salinger, 2020).

The early history of the Cathedral is documented by an architect Hermann Bollé in his work titled „Program Hermana Bolléa, graditeljstva prvostolne crkve zagrebačke, o obnovi te crkve, čitanog u sjednici odbora društva za dogradnju prvostolne crkve, 21. siječnja godine 1884." which translates to „The program of Herman Bollé, the construction of the first Cathedral church in Zagreb, on the renovation of that church, read at the session of the Board of the Society for the extension of the first Cathedral church, on January 21, 1884". In this document Bollé mentions that before the cathedral was built, a smaller church built in a romantic style existed in the location of cathedral. This church was dedicated to the bishop Stjepan I. in 1217 with the presence of the contemporary king Andrija II (Crnković, 1992).

The church eventually became too small due to the increase in population and larger one was built on the same site in the middle of the thirteenth century. As a result of the Tatar campaigns, the church was destroyed in 1242, and it took about three decades for the church to be rebuilt. Bishop Timothy was responsible for the restoration of the cathedral in the Gothic style in the second half of the thirteenth century and tried to build it on the old foundations. For this restauration, a sanctuary, two chapels and a sacristy were built. In the fourteenth century, a fire partly destroyed the cathedral. A new wave of restorations began but were done poorly (Crnković, 1992). In the fifteenth and sixteenth centuries, during the Renaissance, the cathedral received fortification elements, the most famous of which is the Bakač Tower.

In 1646, the Cathedral was engulfed in fire, which destroyed its roof, and the bell tower cracked. In addition to the fire, the cathedral was hit in 1880 by a strong earthquake that was fatal to its bell tower, causing it to crack (Figure 2-1.). Its restoration in the nineteenth century was led by the architect H. Bollé according to a project by Friedrich von Schmidt. Bollé did not stick to Schmidt's project but added a neo-Gothic tone to the cathedral with two tall, spiked towers located on the façade and removed Baroque and Romanesque elements (Salinger, 2020).

Figure 2-1. The Zagreb Cathedral before the earthquake of 1880 (Crnković, 1992).

At the beginning of the twentieth century, there was a lot of controversy about the demolition of the Bakač Tower in 1906. In the same year, Viktor Kovačić founded the Club of Croatian Architects, whose tasks were to protect antiques, to announce public tenders for all buildings of public character, and to enable architects to exhibit their works publicly like other artists (Salinger, 2020).

Between 1937-1941 and 1967-1986 new restorations were done. Original types of stones „Litavac“ and lithothamnium limestone were used. The stone was taken from the „Bizek“ and „Vrapče potok“ quarries. Marić (1938) done extensive examination on the damaged lithothamnium limeston blocks of the Cathedral. It was determined that the primary cause for the surface erosion of this type of limestone was sulphuric acid rain. The samples did not contain gypsum. A black crust and a white powdery material beneath the black crust was seen. The black crust and the white powdery material did contain gypsum (Crnković, 1996). Due to this, Roman travertine was used. Roman travertine resembles the lithothamnium limestone in both colour and appearance, while having superior physical and mechanical properties, like being more durable in polluted atmospheres of an urban environment (Crnković, 1996).

The restoration of the first 40 m gallery happened from 1990 to 1994. Branko Crnković proposed a plan for the restauration of the Zagreb Cathedral. He proposed the replacement of the stone elements as to restore the gallery, and cleaning, fixing and surface protection of dilapidated and damaged stone, which primarily referred to the outer walls of the cathedral. Crnković concluded that alkaline silicates and fluorosilicon compounds should

be used for the fixture of already existing stone. He also concluded that silicone-based preparations should be used for surface protection of newly added stone. The first step was the restauration of the first gallery using the stone called travertine. In this step, two cornices, balusters and a finial were planned to be restored. After that, the adjacent pinnacle would be restored (figure 2-3.) (Crnković 1994).

To conserve the pinnacle as much as possible, 21 drill samples were taken from it (figure 2-2.). The results showed that sulphates were present in the rock, reaching to the depts of 3 to 18 cm in the drill samples. The presence of sulphates did not correlate to the rock's mechanical and physical properties. The sulphates needed to be removed by washing the rock (Crnković, 1994).

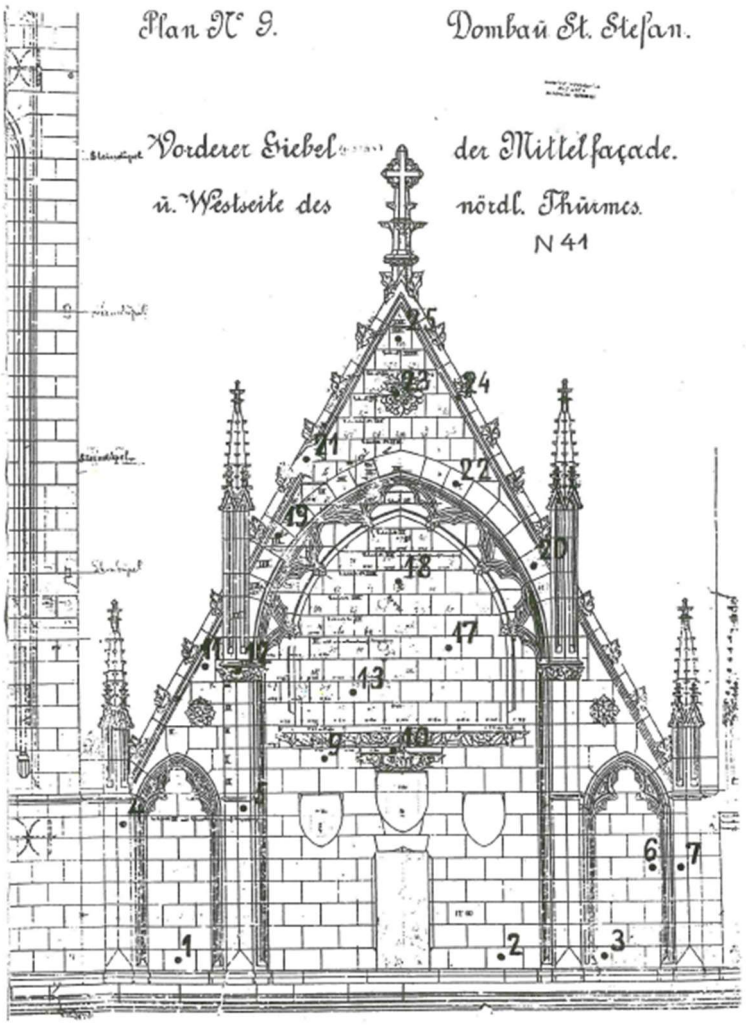

Figure 2-2. Sampling locations of the pinnacle (Crnković, 1994)

Figure 2-3. Pinnacle before and after the restoration (Crnković, 1994)

After that, the work shifted to the gable between the belltowers which was done in 1997. Work was also done on the central part of the western façade and the top of the belltower. Although the goal was to preserve the original elements, this proved fruitless. The gargoyle sculptures, and the statures of Mother of God with Jesus, and two angles need to be replaced. Because the stone from the Zagreb Mountain was not resistant to atmospheric influences, Roman travertine was used for constructive elements. Zagreb Mountain stone was still used for some less exposed elements. „Bizekmort“, a kind of mortar that gives an appearance of old stone from the Zagreb Mountain, was used on surfaces and profiles were not greatly damaged (Crnković, 1996).

In March 2020, the cathedral was hit by a strong earthquake damaging the bell tower on the facade, statics, vault, etc. Repairs and damage assessments are still ongoing, and fragments of the tombstone of Bishop Baratin were found (Salinger, 2020).

As of late 2020, The European Union Solidarity Fund approved 194 million HRK for the proposes of renovating the Zagreb Cathedral. As of January 10th, 2022, approximately 25 tons of material have been removed from the cathedral. In the next phase another 50 tons will be removed, or an additional 10 meters from the very top. Scaffolding in the interior is a temporary solution to the fragility of earthquake-prone structures.The funds will be provided as the works progress, announced the Minister of Culture Nina Obuljen-Koržinek (Narod.hr, 2021).

3. METHODS FOR DETERMINING OF STONE COMPOSITION AND PHYSICAL PROPERTIES

Encyclopaedia Brittanica (Klein, 2021) defines a rock, in geology, as: „a naturally occurring and coherent aggregate of one or more minerals“. A similar term, stone, can be defined as: „a heterogeneous substance characterized by a wide range of mineral compositions, textures, and rock structures“ (Winkler, 1997). Due to this, the physical properties and the durability of rock can vary greatly. Because of this, not all stone is suitable for usage in building. The suitability of a stone for a given building can be tested in the laboratory. This can be done by determining the stone's composition and physical properties.

3.1. X-ray analysis: powder diffraction

X-rays are a form of electromagnetic radiation with the wavelengths of only 10^{-11} to 10^{-8} meters. When an X-ray strikes an atom, the wavelike character of the X-ray causes electrons, protons, and neutrons to vibrate. X-ray wavefronts are produced by the oscillating electrons' reemission of radiation, which leaves the atom in all directions (figure 3-1.). This process, called scattering, is not the same for all elements, nor is it the same in all directions. X-rays propagate in all directions and may exhibit constructive or destructive interference. Due to this, the X-ray energy is more intense where constructive interference is present. This channelling of energy in specific directions is diffraction. Compounds can be recognized by using a database of diffraction patterns because the majority of materials have distinctive diffraction patterns. Instead of using a single crystal, the diffraction pattern in powder X-ray diffraction is derived from the material's powder (Perkins, 2020).

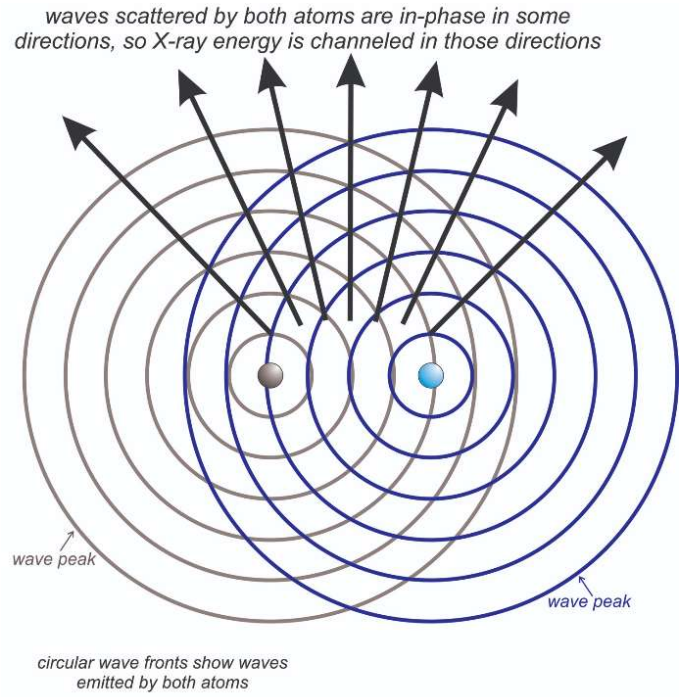

Figure 3-1. Wave interference of two atoms (Perkins, 2020)

An X-ray source (often an X-ray tube), a sample stage, a detector, and a means to vary angle θ make up a powder X-ray diffractometer. (figure 3-2.). A small sample of the mineral is powdered and placed on a glass slide. This is done so the sample can have every possible crystalline orientation represented equally (Dutrow & Clark, 2022). While the detector across from the source measures the intensity of the X-ray it receives at 2θ from the source route, the X-ray is focused on the sample at a variety of θ angles. The detector angle always stays 2θ above the source path while the incidence angle gradually increases (Chemistry Library$_a$, 2020).

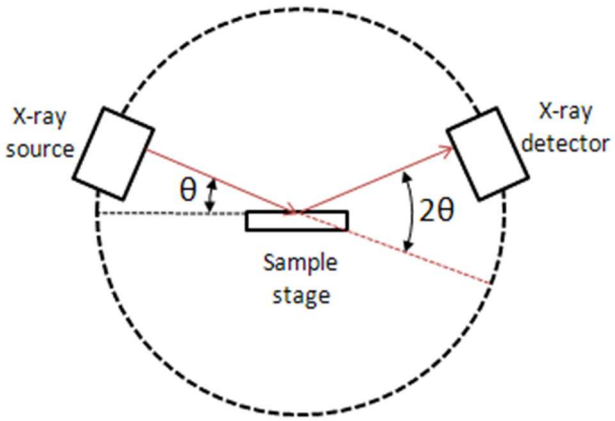

Figure 3-2. Basic X-ray diffractometer setup (Chemistry Library$_b$, 2020)

An X-ray beam is diffracted at an angle of 2θ from the incident beam because the angles of incidence and reflection are equal (figure 3-3.). Diffraction occurs at multiple 2θ angles because a crystal includes numerous atoms that are spaced differently (Perkins, 2020). The incoming beam of these waves is either reflected off the sample's surface or it can enter the sample's lattice and be diffracted by the atoms there. The X-ray that is not scattered passes through to the next layer of atoms, where a part of it is dispersed again and a part of it continues to the next layer (Chemistry Library$_a$, 2020). When the path-length difference 2dsinθ is equal to an integer multiple of the wavelength and the atoms are organized symmetrically with a separation distance d, only then would these waves interfere constructively, according to Bragg's equation, generating a diffraction maximum. (Chemistry Library$_b$, 2020).

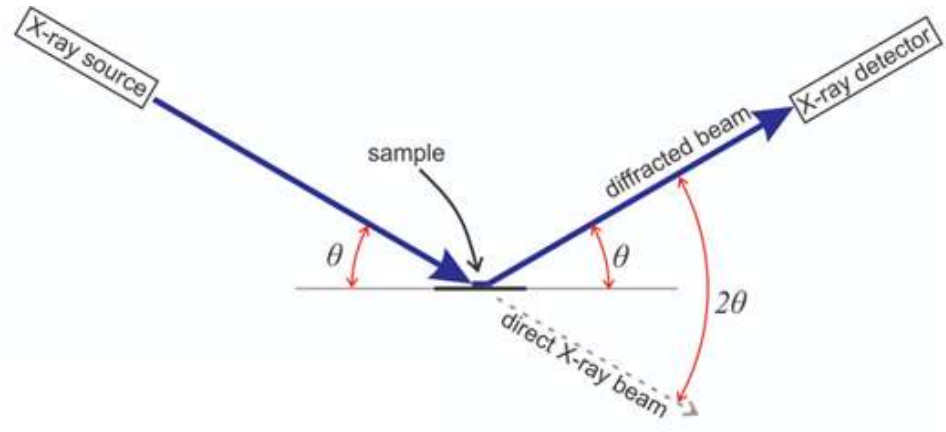

Figure 3-3. Diffraction geometry (Perkins, 2020)

When X-ray is used on a powdered sample; a powder diffraction pattern can be created. When the mineral has lattice planes with the proper d-spacing to diffract X-rays at that value of θ, the intensity peaks. The key information from the pattern is a list of d-values with diffraction intensities (Dutrow & Clark, 2022).

The distance between parallel planes of atoms determines where the diffraction peaks are located (Speakman, 2014).

Each d-value represents sets of planes, and the intensity represents the number of atoms on each plane. The characteristic set of d-spacings generated in a typical X-ray scan provide a unique fingerprint or the mineral present in the sample This is because atomic arrangements change amongst minerals, so they yield different patterns (Flohr, 1997).

X-ray diffraction pattern appears on a computer screen as a sequence of peaks of various heights. These peaks are a product of the crystalline structure and mathematically correlate with atomic spacings between planes of atoms in the material crystal. Next, the computer compares these peaks to the patterns of all minerals that have been recorded.

X-ray powder diffraction (XRD) was performed using a Panalytical Empyrean diffractometer (Bragg-Brentano geometry) (figure 3-4.). Anti-scatter and divergent slit were set at ½ rad, the receiving Soller slits at 0.04 rad and the receiving Soller slits at 0.03 rad. Step size was configured at 0.013°theta/s. XRD was performed between 3° to 70° 2theta on rotating sample stage. XRD analysis was done on the first set of samples (8962-8971) (figure 3-5).

The uneven top parts of the samples were used for X-Ray powder diffraction (figure 3-5.). These parts were used as they needed to be cut anyways to get even, cylindrical samples to determine physical properties on. The cut tops were then beaten down with a hammer as to make them easier to fit into the laboratory mill bowl (figure 3-6.). The mill bowl with the crushed sample was placed in the laboratory mill (figure 3-7.) The samples were then powdered in a laboratory mill (figure 3-8.) and sent to the diffractometer. The results are diffraction patterns which are then analysed using the program called X'Pert HighScore which was used to estimate the stone composition.

Figure 3-4. X-ray powder diffractor used in the study

Figure 3-5. Samples before being powdered

Figure 3-6. Laboratory mill bowls

Figure 3-7. The laboratory mill used to powder the samples

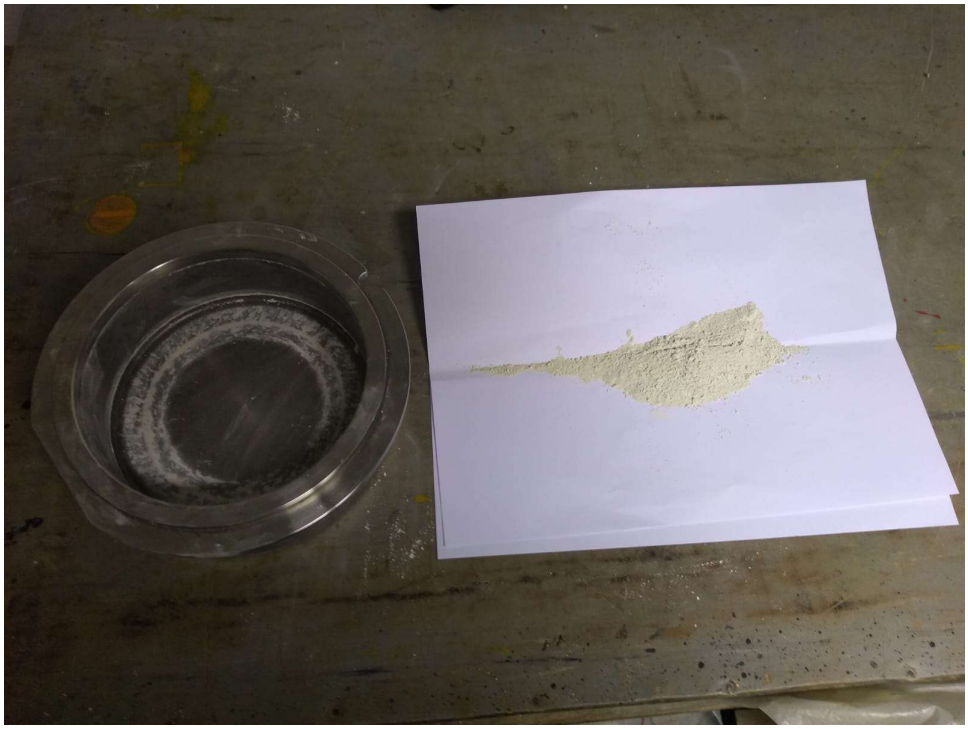

Figure 3-8. Example of a powdered sample used in XRD analysis

3.2. Calcimetry

The calcimeter is basically a Scheibler apparatus. The method is used for determination of carbonate content in the powdered sample and is based on a volumetry (Eijkelkamp Agrisearch Equipment, 2012).

Figure 3-9. Tools used in calcimetry

The calcimeter provides information on total carbonate content in various samples for example in limestone. Samples containing dolomite cannot be determined accurately due to slow reaction rate.

Principle follows: the volume of released carbon dioxide is measured after reaction of dilute hydrochloric acid and the powdered rock samples. First, the calcimeter is calibrated with a fixed amount of 100% calcium carbonate, and the same weight of sample is further used for testing. The carbonates present in the standard or sample react with hydrochloric acid and CO_2 is released.

As a result, the CO_2 is released, and pressure of the gas displace water in the apparatus (figure 3-10.). The volume of displaced liquid is than measured (volumetry). The released quantity of CO_2 is related to the carbonate content by calculation taking in account the reference value of 100 % calcium carbonate.

Figure 3-10. Calcimeter prepared for measurement: tube is filled to zero-mark before the hydrochloric acid reaction with sample and CO_2 release

The procedure of determining the sample mass:

1) starts by filling a reaction vessel with a specific amount of pure calcium carbonate ($CaCO_3$, 0,2 – 0,3 g, determined precisely using analytical balance) (figure 3-11. and figure 3-14.).
2) then the test tube is filled with 4 M hydrochloric acid and placed in the reaction vessel using a pair of tweezers (figure 3-9.).
3) the reaction vessel is closed using the rubber stopper (figure 3-12.) and the whole flask is put onto magnetic stirrer into the measuring position. By tilting

the flask, the hydrochloric acid flows out of the test tube and over the calcium carbonate ($CaCO_3$) starting the reaction.

4) when the reaction is brought to the end the volume of carbon dioxide is measured (figure 3-13.).

Figure 3-11. Pro analysis powdered $CaCO_3$

Figure 3-12. Erlenmeyer flask with a sample and hydrochloric acid, before being tiled

Figure 3-13. Apparatus after the CO_2 release

If the produced volume of the CO_2 is within the reasonable range of calibrated tube of the apparatus, the same mass is used for determination of carbonate content within the samples.

In addition, a blank must be measured. Blank (a baseline) is determined by reaction of hydrochloric acid with 20 ml of distilled water. As no carbonate is added, only the CO_2 dissolved in water is quantified and subsequently subtracted from all measurement that follows (Eijkelkamp Agrisearch Equipment, 2012).

The carbonate content is calculated using following formula:

$$w(CaCO_2) = 1000 \cdot \frac{m_2(V_1 - V_3)}{m_1(V_2 - V_3)} \cdot \frac{100 + w(H_2O)}{100} \quad (3\text{-}1)$$

w (CaCo₃) - the carbonate content of the dried sample (g/kg),

m_1 - the mass of the test portion of the sample (g),

m_2 - the mean mass of the calcium carbonate standard (g),

V_1 - the volume of carbon dioxide produced by reaction of the test portion of the sample (ml),

V_2 - the mean volume of carbon dioxide produced by the calcium carbonate standards (ml),

V_3 - the volume change in the blank determinations (ml),

w (H_2O) - the water content, of the dried sample determined according to ISO 11465 (wt. %) (Eijkelkamp Agrisearch Equipment, 2012).

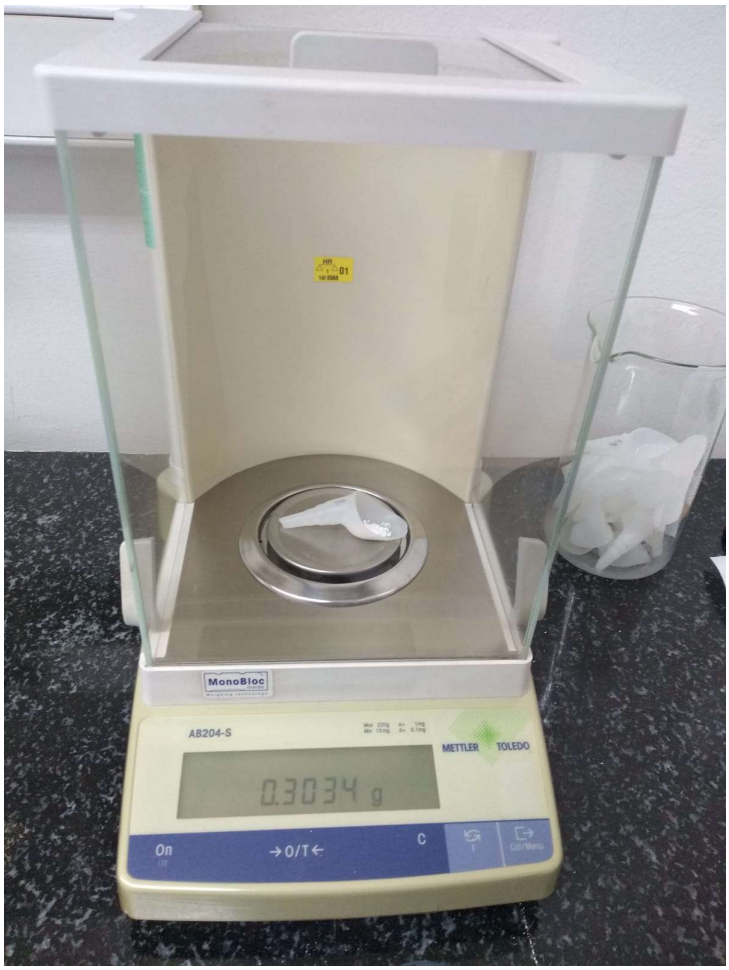

Figure 3-14. Weighing of the mean mass of the calcium carbonate of a sample

The samples with the most ambiguous results in the powder diffraction pattern were selected (6 samples out of 20) and tested to determine total carbonate and the insoluble residue content.

The results were applied to calculate the input masses of original samples sufficient to produce enough insoluble residue to run further XRD analysis.

The chosen samples were: 8963, 8964, 8966, 8968, 8970 and 8971 (figure 3-15.). First the loss by drying was determined. The samples were heated at 105 °C, stored in desiccator to cool and weighted. The samples were dry when their subsequential weight loss was less than 0.1% (wt.).

Around 3 grams of powdered sample was (figures 3.16. and figure 3-17.) left to dry in small crucible (figure 3-18.), cooled and weighted. The water content was calculated using the equation:

$$w = \frac{m_b - m_a}{m_b} \cdot 100 \qquad (3\text{-}2)$$

where:

m_b - mass of the sample and the crucible (before drying) (g),

m_a - mass of the sample and the crucible (after drying) (g),

w - moisture content (%).

Figure 3-15. The powdered samples used for determining the moisture content

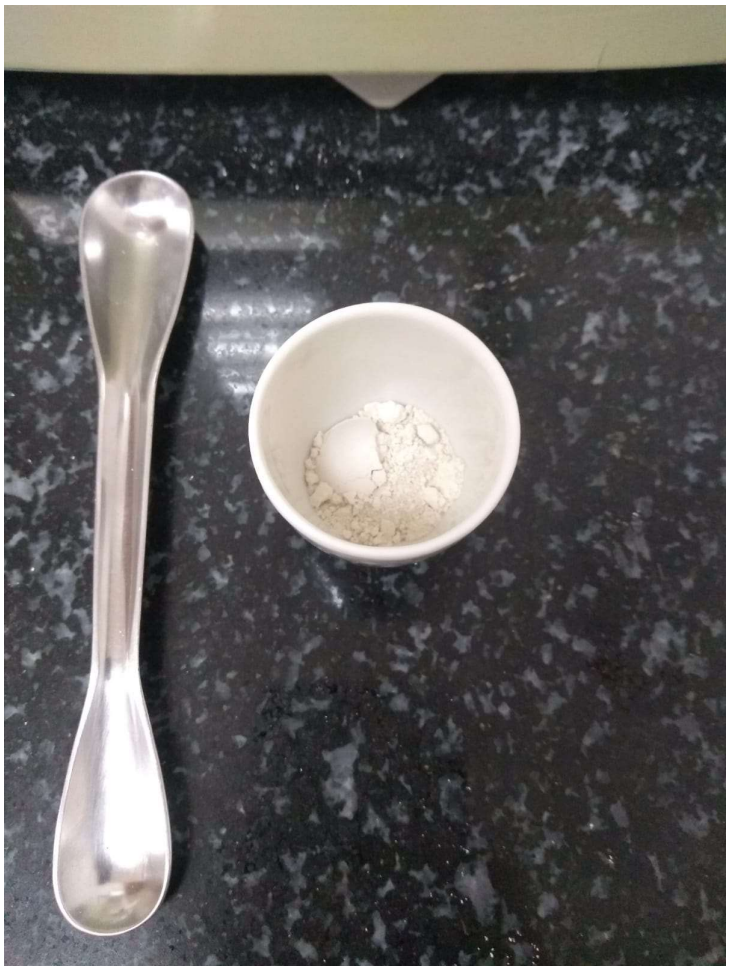

Figure 3-16. The powdered sample in crucible prior the heating

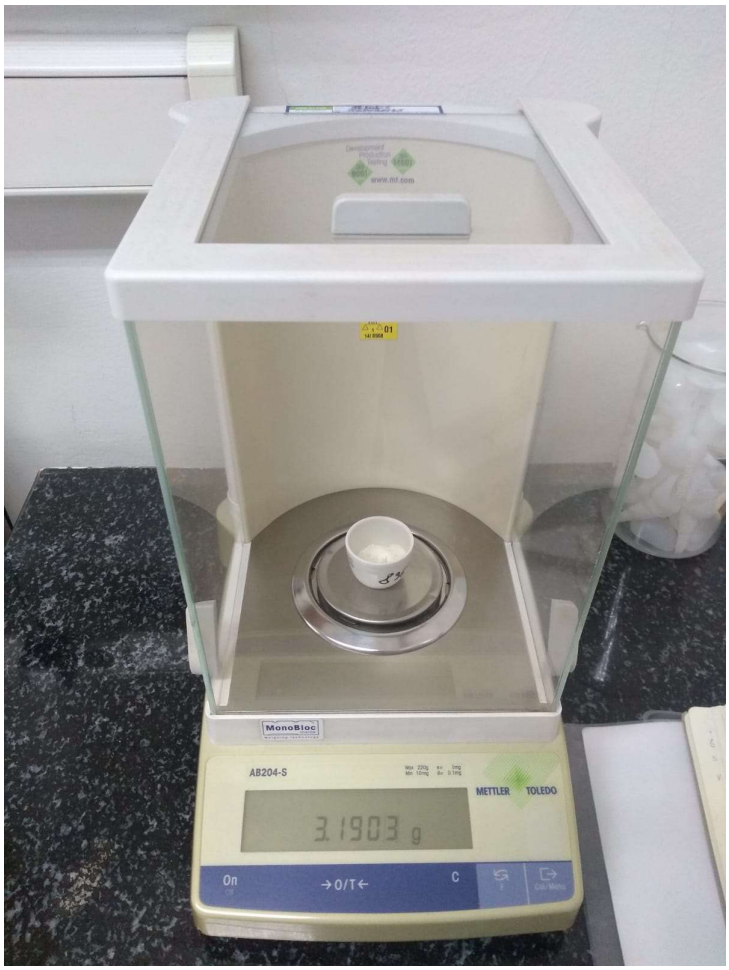

Figure 3-17. Weighing of the powdered sample in crucible (tare function is on)

Figure 3-18. Samples cooling in a desiccator after drying

3.3. Water absorption at atmospheric pressure

Water absorption at atmospheric pressure (A_b) was determined according to the standard HRN EN 13755 „Natural stone test methods – Determination of water absorption at atmospheric pressure“. Two sets of samples (lithothamnium limestone and sandstone), 10 samples per set, were tested. Two samples per a fallen block form the Cathedral were taken. The samples were cylindrical with their height ranging from 53,5 mm to 56,8 mm and their diameter ranging from 53,00 m to 55 mm (figure 3-19. and figure 3-20.). They were also very porous. The first set of samples needed to be submerged for 6 days in total while the second set needed to be submerged for 8 days in total.

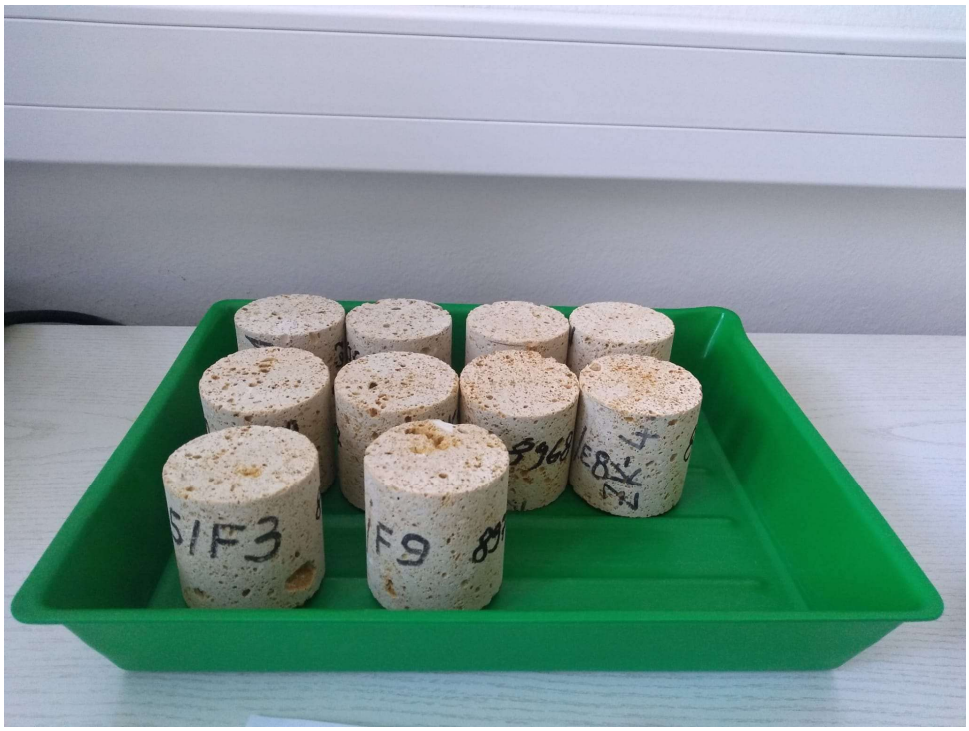

Figure 3-19. First set of samples before drying

Figure 3-20. Second set of samples before drying

Test samples are dried (figure 3-21.) after which their weight is measured (m_d) (figure 3-22.). After drying and measuring the samples and then put into the desiccator, a vessel designed for the removal of moisture from samples (figure 3-23.).

Figure 3-21. Test sample being weighted before drying

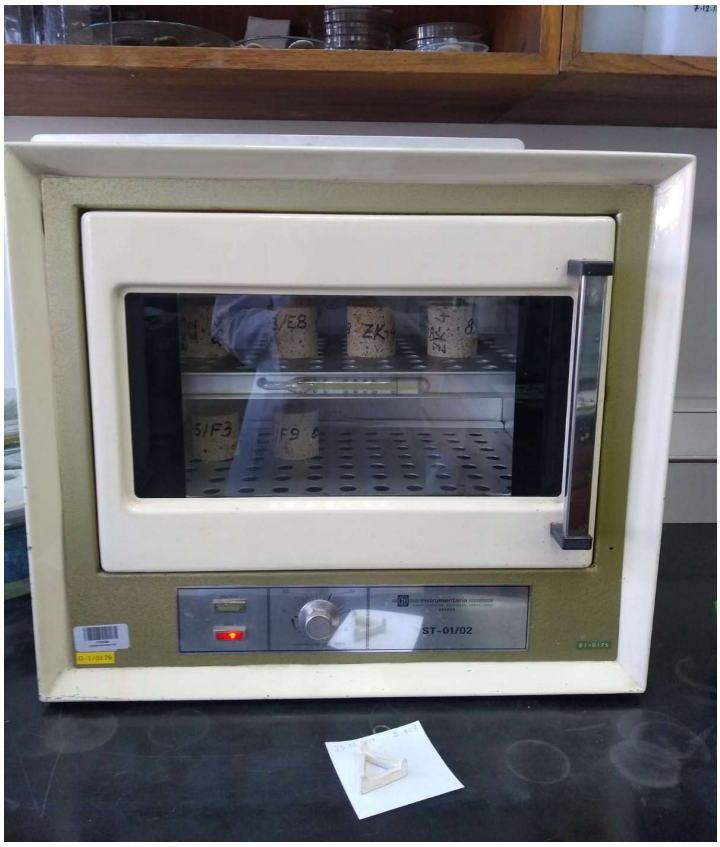

Figure 3-22. Test samples being dried

Figure 3-23. Test samples resting in a desiccator

The samples are then put into a tank with tap water. The tap water must reach half the height of the sample (figure 3-24.).

Figure 3-24. Test samples resting in water half of their height

After an hour, tap water is added until it reaches three-quarter the height of the samples (figure 3-25.).

Figure 3-25. Test samples resting in water 2/3 of their height

After an additional hour, the samples are completely submereged in water (figure 3-26.).

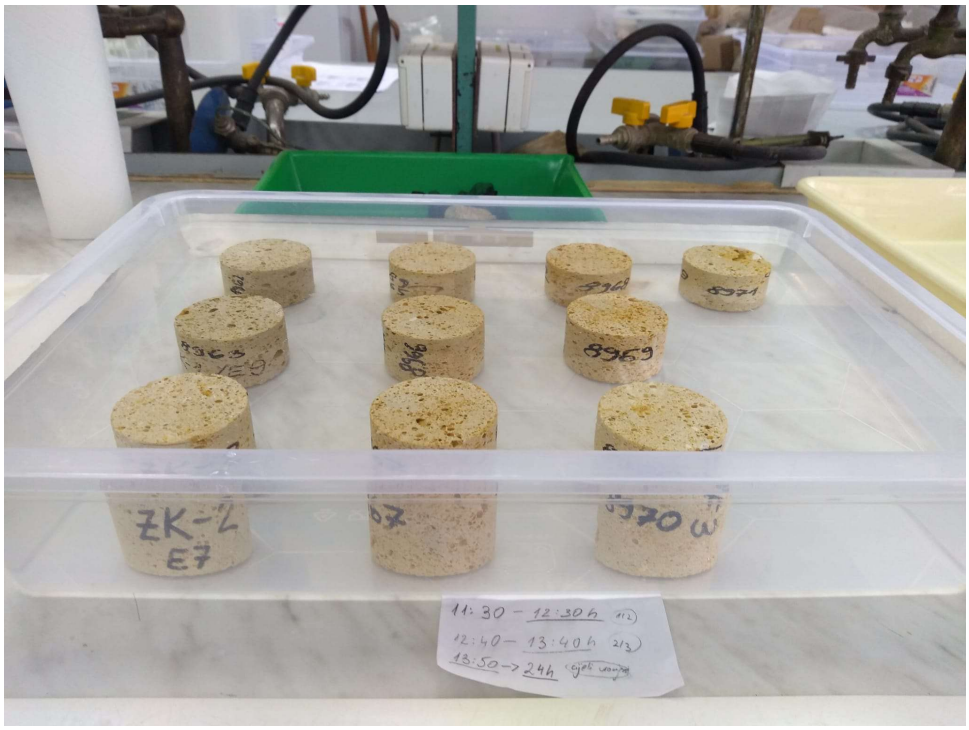

Figure 3-26. Test samples being fully submerged in water

After 48 hours from the initial input of water, the samples are taken out of the water, quickly wiped and weighted within 1 minute (m_i). The sample is then immersed again and weighted every 24 hours (m_i). The test continues until the difference between two successive weightings is not greater than 0.1% of the mass of the sample. The final weightings is the mass of the saturated sample (m_s) (figure 3-27.).

Figure 3-27. A fully saturated sample being weighted

From this, water absorption at atmospheric pressure A_b can be calculated by the equation:

$$A_b = \frac{m_s - m_d}{m_d} \cdot 100 \qquad (3\text{-}2)$$

where:

m_d - mass of the dry sample (g),

m_s - mass of the saturated sample (g),

A_b - water absorption at atmospheric pressure (%).

3.4. Real density

Real density (ρ_r) was determined using the method A (pycnometer) according to the standard HRN EN 1936 „Natural stones test methods – Determination of real density and apparent density, and of total and open porosity (EN 1936:1999)”. All 20 of the samples were tested: 8962-9871 and 9085-9094.

The process stared by measuring the empty pycnometer’s mass and volume (figure 3-28.). The mass of the empty pycnometer was measured 3 times and arithmetic middle was taken. After this, the pycnometer was filled with deionized water. The excess of water left the pycnometer through the ground stopper. After gently wiping the overflow, the final weight of the pycnometer was determined (figure 3-29.). This was done 3 times and the mean value was taken as m_2. This was done for greater precision. From this, the water density was calculated (ρ_{rh}).

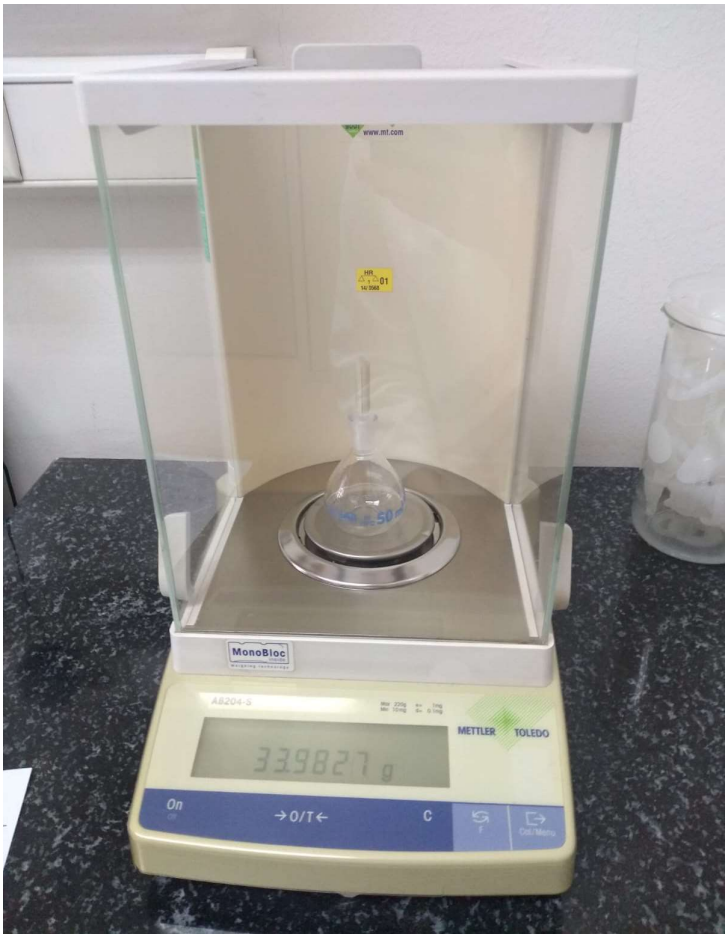

Figure 3-28. Empty pycnometer weighted

After determining the apparent density and open porosity, each sample is grinded until they can pass through a sieve with 0.063 mm mesh. The ground sample is then dried to a constant mass. From this mass, approximately 25 g is taken (m_e). In this study, the samples were hammered to a much larger particle size (around 2 mm). This was done due to the lack of a vacuum pump, so larger sample size was taken. Also, around 1 g of each hammered sample was taken. After that, the pycnometer was filled half-way with only deionized water and its mass was measured.

Then, the 1 g of each hammered sample were put into a pycnometer that was half-way filled with only deionized water. Such samples were put into the half-way filled pycnometer. The rubber stopper was fitted, and the water overflow was gently wiped off. The now-full pycnometer was then weighted 3 times (the mean value being m_1) (figure 3-29.).

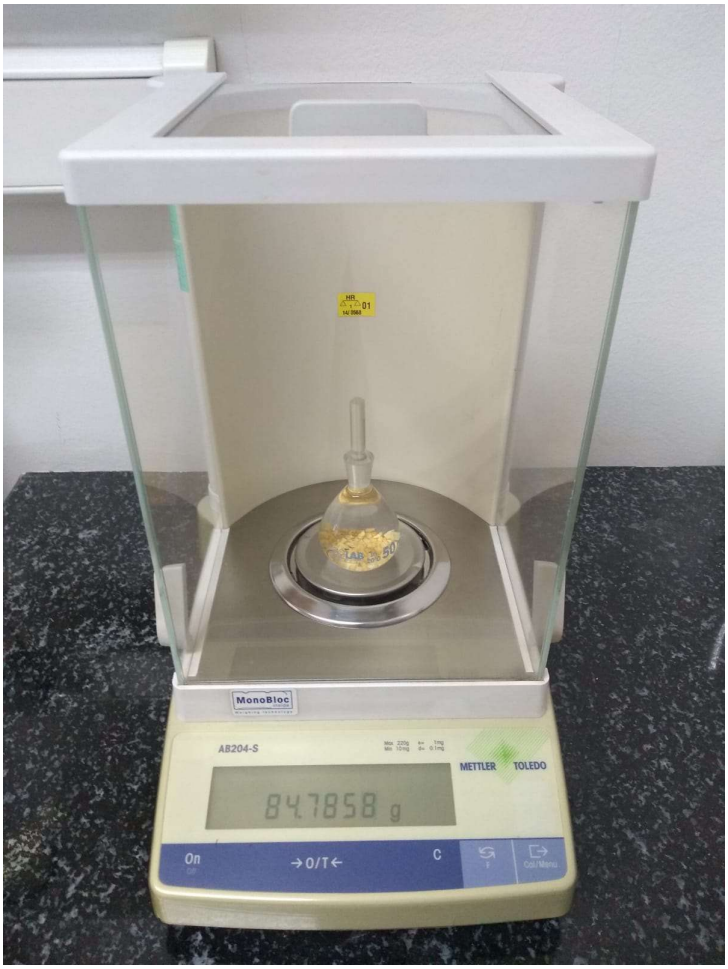

Figure 3-29. Now full pycnometer weighted

From this, the real density of each sample was calculated using the equation:

$$\rho_r = \frac{m_e}{m_2 + m_e - m_1} \tag{3-4}$$

where:

m_e - mass of the sample ground and dried (g),

m_1 - mass of the pycnometer filled with water and the ground sample (g),

m_2 - mass of the pycnometer filled with water (g),

ρ_r - real density of the sample (kg/m^3).

3.5. Open porosity, total porosity, and apparent density

Open porosity (p_o), total porosity (p) and apparent density (ρ_0) were all determined on every sample according to the standard HRN EN 1936 „Natural stones test methods – Determination of real density and apparent density, and of total and open porosity (EN 1936:1999)“. As with determining real density, all 20 of the samples were tested: 8962-9871 and 9085-9094.

Before the testing procedure, each sample needed to be dried at a temperature of (70±5) °C until a constant mass was reached. After an interval of (24±2) h, the samples were weighted. The constant mass was reached when the difference between two weighing was not greater than 0.1% of the mass of that sample. After that mass was reached, the samples were kept in a desiccator to cool down to room temperature.

The test procedure for open porosity and apparent density started by weighing the mass of the dry ground sample (m_d). After this, the samples were submerged in water. After that, the weight of the sample was measured every 24 hours. The weight was measured in two separate ways. The sample was weighted under water (m_h) (figures 3-30. and figure 3-31.) and then the same sample was quickly wiped with a dampened cloth and its mass was determined (m_s) (figure 3-32.). The samples were submerged until the difference in both weights was not greater than 0.1%. Additionally, m_h was always measured in the same depth.

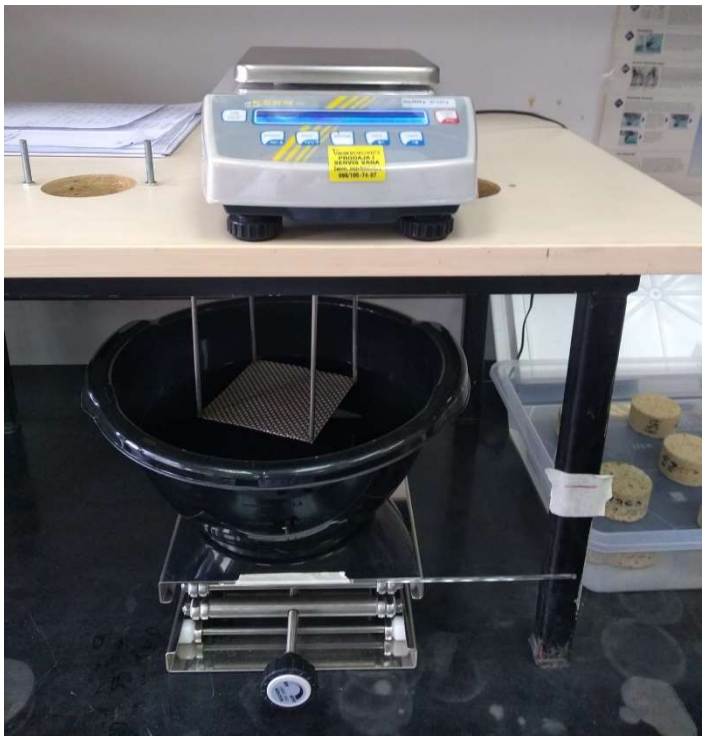

Figure 3-30. The setup for measuring the sample's weight under water (m_h)

Figure 3-31. Sample 8970 being placed on setup for measuring the sample's weight under water (m_h)

Figure 3-32. Sample 8970 weighted after being wiped with a damp cloth

The norm dictates that the density of water (ρ_{rh}) at 20°C is 998 kg/m^3, but the density of water calculated using the pycnometer method was used for more accurate results.

Apparent density was calculated using the equation:

$$\rho_b = \frac{m_d}{m_s - m_h} \cdot \rho_{rh} \tag{3-5}$$

where:

m_d - mass of the dry sample (g),

m_h - mass the sample immersed in water (g),

m_s - mass of the saturated sample (g),

ρ_{rh} - density of water (kg/m^3),

ρ_b - real density of the sample (kg/m^3).

From this, open porosity was calculated using the equation:

$$p_o = \frac{m_s - m_d}{m_s - m_h} \cdot 100 \tag{3-6}$$

where:

p_o - open porosity of the sample (%).

Additionally, open porosity could be calculated using the ratio of the volume of open pores and the apparent volume of the sample.

The volume of open pores was calculated as:

$$Vo = \frac{m_s - m_d}{\rho_{rh}} \cdot 1000 \tag{3-7}$$

where:

V_o - volume of open pores of the sample (ml).

The apparent volume of each sample was measured using a calliper, but it was also calculated to see if there was any difference between the two results. The equation for apparent volume goes as following:

$$V_b = \frac{m_s - m_h}{\rho_{rh}} \cdot 1000 \tag{3-8}$$

where:

V_b - apparent volume of the sample (ml).

Also, the open porosity can be calculated using the equation:

$$p_o = \frac{V_0}{V_b} \cdot 100 \tag{3-9}$$

Total porosity was expressed by the ratio (percentage) of the volumes of pores and the apparent volume of the sample, using the equation:

$$p = \frac{\frac{1}{\rho_b} - \frac{1}{\rho_r}}{\frac{1}{\rho_b}} \cdot 100 = \left(1 - \frac{\rho_b}{\rho_r}\right) \cdot 100 \tag{3-10}$$

where:

p - total porosity of the sample (%).

3. ZAGREB CATHEDRAL'S CONSTRUCTION STONE

A Romanesque church was built on the site of today's cathedral in Zagreb in 1217 but was later destroyed by the Tatars. In the middle of the 13th century, a sanctuary was rebuilt on the site, with two chapels and a sacristy in the early Gothic style. After the fire that destroyed the cathedral in the 14th century, it was rebuilt in the late Gothic style. Herman Bollè, who led the reconstruction of the cathedral after its destruction in the earthquake of 1880, to save on the cost of transporting stone, restored the cathedral mostly with stone from the quarry in Vrapče stream, and only partially with stone from Podsused (Bizek), Vinica (near Varaždin) and Bregovo (near Samobor). Along with the new stone, the stone of the ruined cathedral was also installed. The stone used from Bregovo, Vrapče Potok and Podsused (Bizek) is lithothamnium limestone. The stone from Vinica, today known as „Vinicit", is a soft, porous, and easily workable limestone (Crnković; a, 1993). The cathedral was renovated in 1938 and 1968, and lithothamnium limestone was used both times for the renovation. The cathedral has been renovated many times in the past and that continues to the present day.

On March 22, 2020, an earthquake measuring 5.5 on the Richter scale destroyed the top of the cathedral's south bell tower (Prirodoslovno-matematički fakultet u Zagrebu, 2022).

The top of the north tower of the Zagreb Cathedral, 13 and a half meters high and weighing 30 tons, was removed by a controlled explosion (with the help from the Faculty of Mining, Geology and Petroleum Engineering) on April 17, 2020, because due to the damage it suffered in a strong earthquake, there was a danger of it collapsing and damaging the surrounding area. The cathedral tower was separated between the 72nd and 73rd rows, removed by a 500-ton crane, and another crane covered the entire bell tower and lowered it in one piece (Ministarstvo obrane Republike Hrvatske, 2020).

The cathedral was further damaged in the earthquake that occurred on December 29 with the epicentre near Petrinja (Informativna katolička agencija, 2020).

Lithothamnium limestone is primarily made of red algae of the genus *Lithothamnium*, which thrived in the Paratethys Sea at the time, fifteen million years ago,

during the Middle Miocene. Lithothamnium limestone is a highly porous kind of limestone (Crnković, 1996 & Fio Firi & Maričić, 2020).

It was formed in the Pannonian Sea's shallows, which at the time were islands that included Medvednica and other mountains in Pannonian Croatia. Many organisms with a hard exoskeleton and algae, especially of the genus *Lithothamnium*, lived in this sea. Lithothamnium limestone also includes calcite, mica, quartz, and rock pieces found in the coastal areas in addition to the remains of marine organisms. With the development of *Lithothamnium* algae along the entire coast of the shallow Miocene Sea at the foot of Medvednica and with their death, the possibility of the formation of a sediment of carbonate composition called „Lithothamnium limestone“ after the name of the algae was achieved (Marić, 1938). The „primary“ deposits of lithothamnium limestone are deposited on the bedrock and regularly begin with basal breccias and conglomerates that in the southwestern part of Medvednica, mostly contain small fragments of the Lower Triassic dolomites. Lithothamnium limestone rich in limestone exoskeleton of algae and other organisms was deposited on them. The destruction of these „primary“ formations and the deposition of newly formed mineral products in the immediate vicinity resulted in „secondary“ deposits of lithothamnium limestone, which have a pronounced stratification (Crnković; a, 1993). At the foot of Medvednica, deposits of lithothamnium limestone are up to 40 m thick. „Primary“ Lithothamnium limestone can be seen at these sites and in the mentioned quarries. In the recent past, „secondary“ deposits have been used for cement production.

During the first restoration in 1938, Luka Marić investigated and described the damage to the lithothamnium limestone from the Zagreb Cathedral and stated that the stone lost its original appearance and shape, and that severe damage cracking and breakage of smaller or larger parts of the stone elements could be observed. Despite this, the fresh samples of lithothamnium limestone taken right from a quarry showed that the stone is durable and stable enough to be used in building and decorating according to the norms of the time (Marić, 1938). Because of this, lithothamnium limestone was used to reconstruct the cathedral. Marić also noted that lithothamnium limestone embedded on the outside of the cathedral is subject to rapid changes that are more dependent on the atmospheric conditions of the city of Zagreb than on the quality of lithothamnium limestone. Several samples were tested to establish the influence of vegetation (algae and fungi) on stone

destruction, but no link was found. Therefore, mineralogical-petrographic, and chemical tests were performed. Microscopic and chemical analysis indicated that gypsum was present.

There is no trace of gypsum in the fresh lithothamnium limestone from the quarry, so Marić (1938) linked the formation of gypsum to the chemical action of the sulfuric acid atmosphere. Today's condition of the stone of the Zagreb Cathedral is such that a complete renovation is needed. The damage to the stone gallery of the Zagreb Cathedral is the result of the effects of temperature changes (heating and freezing of water in the pore space) and the effects of the „urban atmosphere".

5. THE RESULTS OF THE ZAGREB CATHEDRAL'S STONE ANALYSIS

In this chapter, the results of X-Ray Diffraction and calcination on the first set of samples (8962-8971) will be presented. In addition, results of physical properties of two different sets of samples were presented. The first set of samples consisted of 10 lithothamnium limestone samples (8962-8971), and the second set of samples consisted of 10 sandstone samples (9085-9094).

5.1. The results of X-ray diffraction

The results of the X-Ray Diffraction were determined using the X'Pert HighScore program simulation. With this program, the user can enter a data base of different diffraction patterns for different minerals and find which one best fits the diffraction pattern measured during the X-Ray Diffraction. The results of XRD analysis of 10 samples are listed in the table 5-1. while the diffraction patterns are shown in figure 5-1. and figure 5-2..

Main mineral present in all 10 samples is calcite (figure 5-1. and table 5-1.). There were also a significant amount of dolomite, quartz, and micaceous minerals in all samples. Plagioclase is present in 8966 and 8968 samples while K-feldspars could not be confirmed. 14 Å phyllosilicates were present in the samples 8963, 8966, 8968, and possibly present in samples 8964, 8970 and 8971. 14 Å phyllosilicates include smectite and vermiculite while chlorite was grouped with kaolinite due to their similar diffraction pattern. Goethite and hematite were grouped for the same reason. Kaolinite and/or chlorite were present in the samples 8963,8964, 8966,8968, 8970 and 8971. Goethite was present in the samples 9864,

8966, 9868, 8970 and 8971 while hematite was present only in the sample 8968. Rutile was present only in the specimen 8963. Amorphous substance was probably present in all 10 samples, but it could not be proved since it does not leave any diffraction peaks. The percentage of calcite was estimated for the insoluble residue of six samples (8963, 8964, 8966, 8968, 8970 and 8971) that were put in acetic acid (figure 5-3.). The samples were put into acid as to dissolve the carbonates. Calcite and dolomite were grouped due to both being carbonates. Based on the percentage of mass lost, the ratio between calcite and dolomite could be estimated for those six samples (table 5-1.). Sample 8963 had the least amount of carbonates (around 76%) and samples 8964 and 8971 had the most carbonates (around 94%). It was also determined that dioctahedral phyllosilicates were present.

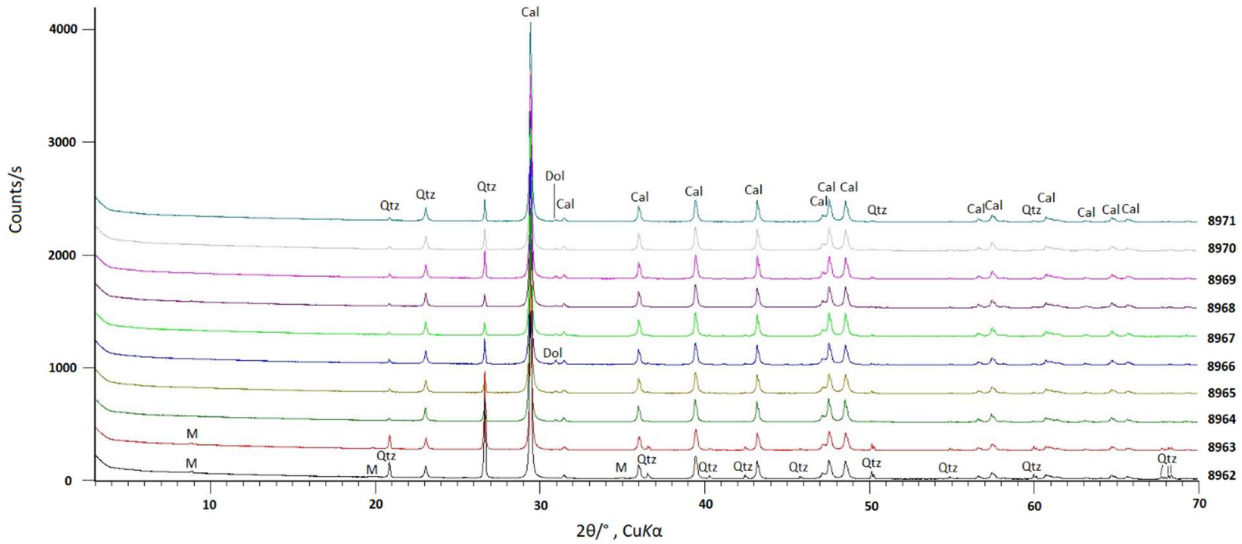

Figure 5-1. The initial diffraction pattern for samples 8961-8971

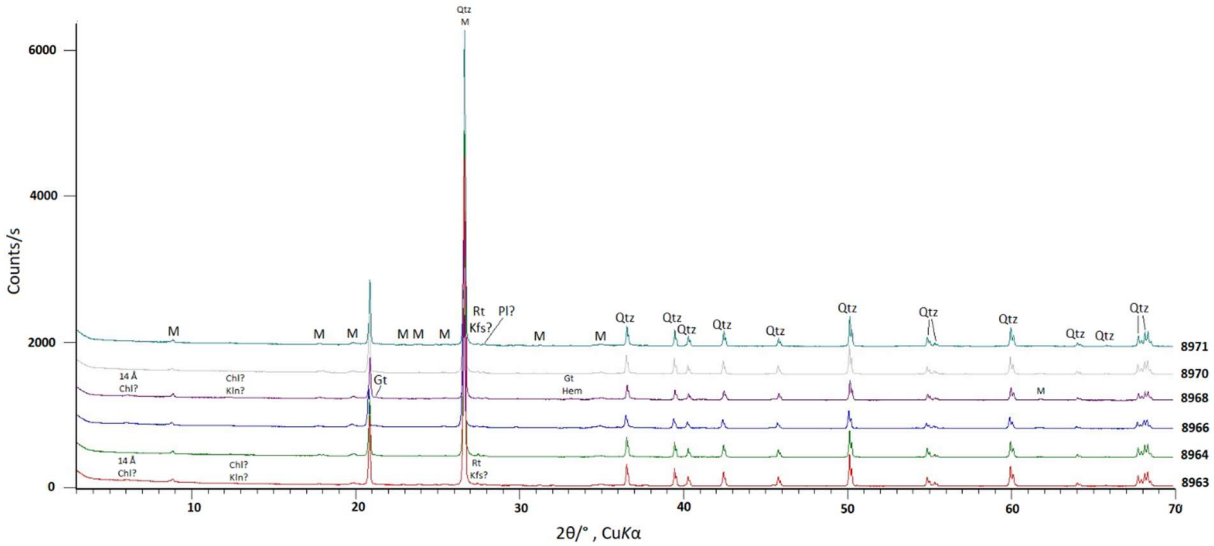

Figure 5-2. The diffraction pattern of insoluble residues for samples 8963, 8964, 8966, 8968, 8970 and 8971

Table 5-1. The results of the initial X-Ray Diffraction of the whole samples

Sample number	Cal	Dol	Qtz	Pl	Kfs	M	14 Å	Kln and/or Chl	Gt	Hem	Rt	A
8962	d	?	++	?	?	++	-	?	?		?	?
8963	d	+	+/++	?	?	++	+	+	?		+	?
	76%											
8964	≥ 90%	+	+	?	?	+	?	+	+	?	?	?
	94%								+			
8965	d	+	+	?	-	?	-	-	-		-	?
8966	> 85%	+/++	+	+	?	+	+	+	+	?	?	?
	92%								+			
8967	d	+	+	-	-	+	-	-	?		-	?
8968	≥ 90%	+	+	+	?	+	+	+	+	+	?	?
	93%								+			
8969	d	+	+	?	?	+	-	?	?		?	?
8970	≥ 90%	+	+	?	?	+	?	+	+	?	?	?
	93%								+			
8971	≥ 90%	+	+	?	?	+	?/+	+	+	?	?	?
	94%								+			

Where:

+	(0-5%)	s	(10-20%)
++	(5-10%)	d	(>20%)

Cal – calcite
Dol – dolomite
Qtz – quartz
Pl – plagioclase
Kfs – K-feldspar
M – micaceous minerals
A – amorphous substance

Kln – kaolinite
Chl – chlorite
14 Å – 14 Å phyllosilicates (smectite and vermiculite)
Gt – goethite
Hem – hematite
Rt – rutile

In addition to the XRD analysis insoluble residue of samples (figure 5-3.) were looked under a loupe and photographed. According to the Munsell soil colour chart, the sample colours were (figure 5-3.):

8963 – 2.5Y 8/2 (pale yellow)

8964 – 2.5Y 7/4 (pale yellow)

8966 – 10YR 7/3 (very pale brown)

8968 – 7.5YR 6/6 (reddish yellow)

8970 – 2.5Y 7/4 (pale yellow)

8971 – 2.5Y 7/4 (pale yellow)

Figure 5-3. Insoluble residues after dissolving the carbonates in acetic acid

Another indicator for the presence of goethite in the samples (9864, 8966, 9868, 8970, 8971) was the light yellowish colour of the insoluble residues (figure 5-3. and figure 5-4.). While insoluble residue of the sample 8968 has the more reddish colour which could be indicator of hematite presence.

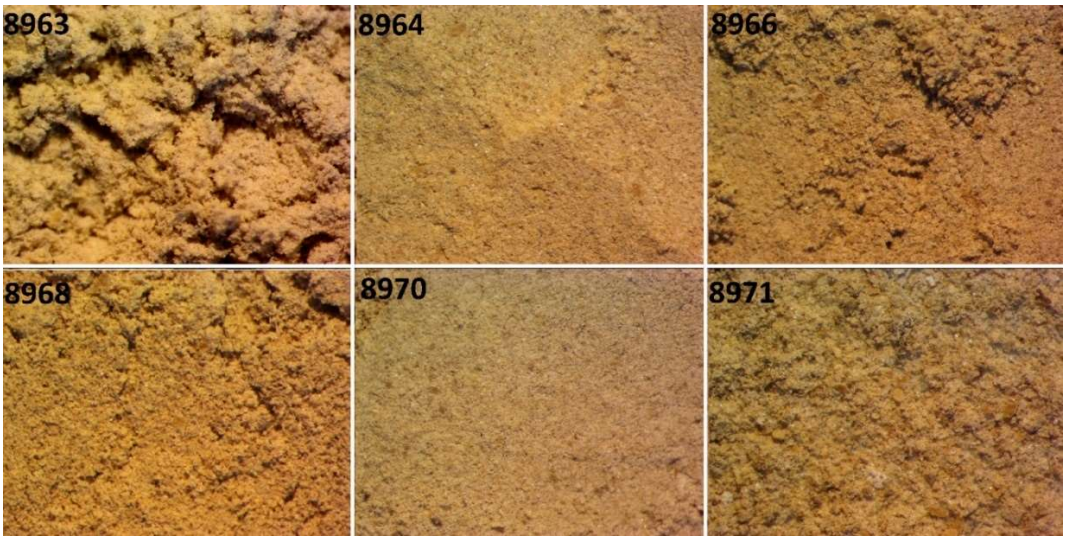

Figure 5-4. The microphotograph of the insoluble residues, 16 times enhanced

After that X-ray diffraction was performed on the insoluble residues. The results are shown in table 5-2. and figure 5-1..

Table 5-2. The results of the X-Ray Diffraction of the insoluble residues

Sample number	Qtz	Pl	Kfs	M	14 Å	Kln and/or Chl	Gt	Hem	Rt	A
8963	d	?	?	s/d	s		?		+	?
8964	d	?	?	s/d	++/s		+	?	+	?
							+			
8966	d	+	?	s/d	d		+/++	?	+	?
							+/++			
8968	d	+	?	s/d	d		++	+	?	?
							++/s			
8970	d	?	?	s/d	++/s		+	?	?	?
							+			
8971	d	?	?	s/d	s		+	?	+	?
							+			

In the insoluble residues, quartz was the most dominant mineral (table 5-2.). Plagioclase was proven to be present in only the samples 8966 and 8968 while K-feldspars were not confirmed to be present in any of the insoluble residues. 14 Å phyllosilicates and kaolinite and/or chlorite were grouped together because their peaks overlapped so they could not be confidently separated. 14 Å phyllosilicates and kaolinite and/or chlorite were dominant in the specimens 8966 and 8968. Goethite was confirmed to be present in all the insoluble residues except for the sample 8963. Goethite and hematite were grouped together for the sample 8963 due to both having very weak diffraction peaks. The sample 8963 also had the palest insoluble residue of all the samples (figure 5-3.). Hematite was only proven in the insoluble residue of the sample 8968. Rutile was not proven only in the insoluble residues of samples 8968 and 8970 but might be present in small quantities. Amorphous substance is probably present in all the insoluble residues.

5.2. The results of calcination

Due to the high percentage of calcite in the samples, it was hard to interpret the percentage of other potential minerals in the samples. Because of this, the X-Ray Diffraction was repeated on six samples that gave the most distinct results during the initial X-Ray Diffraction. During calcination the percentage of the carbonate in each chosen sample was determined (table 5-3.) but also if samples were viable candidates for the carbonate dissolving due to having limited amount of each powdered sample. The samples 8963 and 8964 were chosen because they possibly had the least amount of dolomite while 8966 potentially had the most amount of dolomite out of all the samples. The sample 8968 was similar in the composition to 8966 while 8970 and 8971 samples most likely contain K-feldspars and/or mica. The table 5-3. shows the results of the total calcium content (W) as the content of calcium within a sample compared to the other minerals. In addition, moisture of the samples (w) is the percentage of water by weight of sample. The total calcium content (W) is the content of calcium within a sample compared to the other minerals.

Table 5-3. Moisture (w) and total calcium content (W)

Sample number	w [%]	W ($CaCO_3$) [%]
8963	0.35	76.42
8964	0.16	85.15
8966	0.23	81.88
8968	0.21	84.60
8970	0.13	93.33
8971	0.17	92.67

According to gained results (table 5-3.) all six samples have a high total calcium content. It warried from 76.42% to 93.33%. The samples 8970 and 8071 were especially rich in $CaCO_3$. Regarding moisture content (table 5-2.), it ranged from 0.13 to 0.35%. Samples 8963 had the highest water content (0.35%) while the sample 8970 had the lowest one (0.13%).

5.3. The results of the real density of the samples

Firstly, the weight and the volume of the pycnometer was measured. Two pycnometers were used, one being used only to test the first set of samples (8962 – 9871), while the other was used in testing of the second set of samples (9085 – 9094). After that, the mass of the pycnometer with water was measured. From this, the density of the water could be calculated as:

$$\rho_{rh} = \frac{(m_2 - m_p)}{V_p} \tag{5-1}$$

where:

m_p - mass the empty pycnometer (g),

V_p - volume of the pycnometer (ml).

After that, around 1 gram of each sample was taken and put into a pycnometer filled with water giving data about the weight of the sample, water, and the pycnometer combined. From this, the mass of the water could be calculated (Equation 5-2):

$$m_w = m_1 - m_e - m_p \tag{5-2}$$

where:

m_w - mass of the water in the pycnometer (g),

m_e - mass of the specimen ground and dried (g).

After that, the volume of water could be calculated as:

$$V_w = \frac{m_w}{\rho_{rh}} \tag{5-3}$$

where:

V_w - volume of the water in the pycnometer (ml).

Furthermore, the volume of the sample could be calculated as:

$$V_u = V_p - V_w \tag{5-4}$$

where:

V_u - volume of the sample (ml).

Finally, the real density could be calculated as:

$$\rho_r = \frac{m_u}{V_u} = \frac{m_e}{m_2 + m_e - m_e} \cdot \rho_{rh} = \frac{m_e}{V_s} \cdot \rho_{rh} \tag{5-5}$$

where:

V_s - volume of liquid displaced by the mass m_e (ml),

ρ_r - real density of the sample (kg/m^3).

Density of water for the first set of samples was 996.2 kg/m^3 (table 5-4.) and the real density of the first set of tested samples (8962-9871) ranges from 2327.8 kg/m^3 to 2535.1 kg/m^3 (table 5-5.). The real density of the second set of samples (samples 9085-9094) ranges from 2349.2 kg/m^3 to 2504.3 kg/m^3 (table 5-7.) and the water density was 995.8 kg/m^3 (table 5-6.).

Table 5-4. Calculation of water density of the first set of samples

V_p [ml]	m_p [g]		m_2 [g]		ρ_{rh} [g/cm^3]
50.399	33.9826	33.9827	84.1919	84.1915	0.9962
	33.9827		84.1915		
	33.9828		84.1912		

Table 5-5. Calculation of real density of the first set of samples

Sample number	m_e [g]	m_1 [g]		m_w[g]	V_w [ml]	V_u [ml]	ρ_r [g/cm^3]
8962	1.0087	84.7902	84.7897	49.7983	49.9869	0.4121	2.4476
		84.7896					
		84.7892					
8963	1.0009	84.7892	84.7892	49.8056	49.9942	0.4048	2.4728
		84.7893					
		84.7891					
8964	1.0057	84.7937	84.7936	49.8052	49.9939	0.4051	2.4824
		84.7937					
		84.7935					
8965	1.0030	84.7856	84.7853	49.7996	49.9883	0.4107	2.4419
		84.7853					
		84.7851					
8966	1.0028	84.7961	84.7959	49.8104	49.9991	0.3999	2.5074
		84.7959					
		84.7957					
8967	1.0038	84.8004	84.8002	49.8137	50.0023	0.3967	2.5306
		84.8001					
		84.8000					
8968	1.0022	84.7810	84.7808	49.7959	49.9845	0.4145	2.4179
		84.7808					
		84.7806					
8969	1.0077	84.8035	84.8032	49.8128	50.0015	0.3975	2.5351
		84.8033					
		84.8029					
8970	1.0088	84.7686	84.7686	49.7771	49.9656	0.4334	2.3278
		84.7686					
		84.7686					
8971	1.0087	84.7961	84.7961	49.8047	49.9933	0.4057	2.4865
		84.7961					
		84.7961					

As for the second set of samples, the water density that day was 995.8 kg/m^3 (table 5-6.) and the real density of the tested samples ranged from 2349.2 kg/m^3 to 2504.3 kg/m^3 (table 5-7.).

Table 5-6. Calculation of water density of the second set of samples

V_p [ml]	m_p [g]		m_2 [g]		ρ_{rh} [g/cm^3]
49.730	33.6783	33.67847	83.2011	83.2007	0.9958
	33.6786		83.2006		
	33.6785		83.2005		

Table 5-7. Calculation of real density of the second set of samples

Sample number	m_e [g]	m_1 [g]		m_{vw}[g]	Vw [ml]	V_u [ml]	ρ_r [g/cm^3]
9085	1.0025	83.7933	83.7933	49.1123	49.3183	0.4117	2.4351
		83.7934					
		83.7931					
9086	1.0040	83.7793	83.7791	49.0967	49.3026	0.4274	2.3492
		83.7792					
		83.7789					
9087	1.0077	83.7922	83.7921	49.1059	49.3119	0.4181	2.4101
		83.7920					
		83.7920					
9088	1.0017	83.7902	83.7899	49.1098	49.3158	0.4142	2.4182
		83.7900					
		83.7896					
9089	1.0045	83.8059	83.8058	49.1228	49.3289	0.4011	2.5043
		83.8059					
		83.8056					
9090	1.0052	83.7973	83.7974	49.1138	49.3198	0.4102	2.4504
		83.7975					
		83.7975					
9091	1.0048	83.7803	83.7801	49.0969	49.3028	0.4272	2.3521
		83.7803					
		83.7798					
9092	1.0041	83.8002	83.8004	49.1179	49.3239	0.4061	2.4726
		83.8005					
		83.8006					
9093	1.0003	83.8001	83.8003	49.1215	49.3276	0.4024	2.4857
		83.8007					
		83.8001					
9094	1.0012	83.7966	83.7964	49.1167	49.3228	0.4072	2.4585
		83.7963					
		83.7963					

5.4. The results of determining the water absorption at atmospheric pressure

The value of water absorption at atmospheric pressure for the first set of lithothamnium limestone samples differed from sample to sample (figure 5-5.), but the general pattern was the same. The average water absorption at atmospheric pressure of the samples ranged from 2.32 % in the sample 8966 to 6.02% in the sample 8963 (table 5-8.). This was a range of 3.7%. The final average water absorption at atmospheric pressure for all 10 samples was 3.46%. All the samples (excluding the sample 8962) showed a sharp increase in water absorption after an initial couple of hours of being fully submerged in water (from 210 to 330 minutes). And after that, the water absorption tended to slightly increase in intensity, excluding the samples 8963 and 8968. A decrease in the water absorption could be seen on the samples after 1140 minutes (about 19 hours), as probably an error during measuring that day. After that 19-hour mark, all the samples saw a stagnating increase or a slight decrease in water absorption up to the 9000-minute mark (or about 6 days). Compared to the initial rise in water absorption, the samples 8963 and 8968 show a decrease in value of water absorption. The rest of the samples show a steady increase in water absorption compared to the initial value of water absorption.

Table 5-8. The water absorption at atmospheric pressure of the first set of samples

	A_b [%]							
Sample number	A_b 210 min [%]	A_b 270 min [%]	A_b 320 min [%]	A_b 1440 min [%]	A_b 2880 min [%]	A_b 4320 min [%]	A_b 8640 min [%]	A_b average [%]
8962	5.52	5.55	5.56	5.53	5.67	5.69	5.69	5.60
8963	6.12	6.23	6.23	5.81	5.90	5.91	5.94	6.02
8964	2.23	2.40	2.40	2.30	2.53	2.48	2.49	2.41
8965	2.23	2.56	2.63	2.74	2.82	2.79	2.77	2.65
8966	2.04	2.22	2.31	2.27	2.46	2.46	2.46	2.32
8967	2.54	2.68	2.70	2.66	2.85	2.91	2.93	2.75
8968	4.19	4.32	4.34	3.93	3.93	4.01	4.10	4.12
8969	2.36	2.68	2.68	2.62	2.68	2.76	2.79	2.65
8970	2.45	2.61	2.64	2.57	2.66	2.66	2.66	2.61
8971	3.68	3.88	3.93	3.90	3.93	3.90	3.94	3.88
Average	3.34	3.51	3.54	3.43	3.54	3.56	3.58	3.46

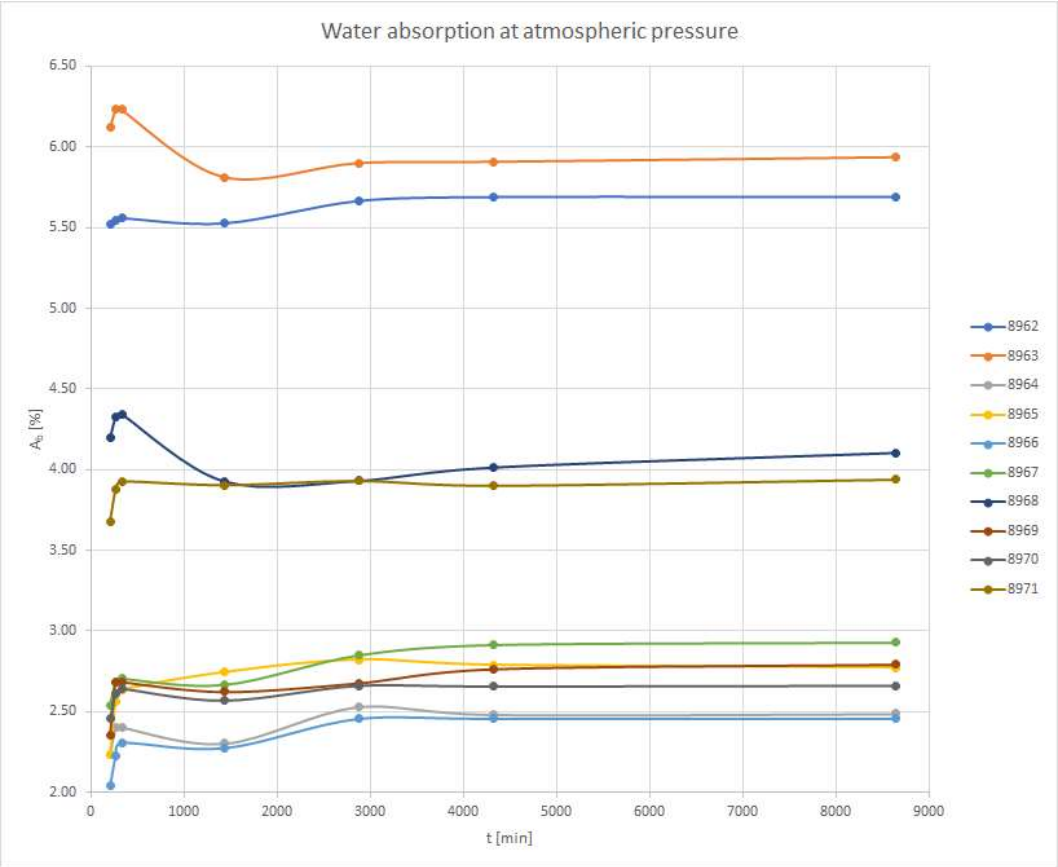

Figure 5-5. Graphical presentation of the water absorption at atmospheric pressure of the first set of samples

Regarding the second set of samples (table 5-9.), they show a steady increase in water absorption until hitting the 4320-minute mark (3 days). After that, the water absorption was still rising, but more slowly, growing less than 0.1% after 11520-minute mark (8 days) (figure 5-6.). The second set of samples might have taken longer to achieve its final saturated weight due to possessing higher values of porosity compared to the first set of samples. The mean water absorption of the samples ranged from 6.20% in the sample 9089 to 11.34% in the sample 9092. This was a range of 5.14%. The final average value for water absorption at atmospheric pressure was 9.56%. This means that the second set of samples had a higher water absorption than the first set of samples. The maximum mean water absorption of the first set of samples (6.02%) was lower than the minimum mean water absorption of the second set of samples (6.20%). The difference between the lowest mean water absorption and the highest mean water absorption from both sets of samples (2.32%-11.34%) gives the range of the mean water absorption of 9.02%.

Table 5-9. The water absorption at atmospheric pressure of the second set of samples

	A_b [%]									
Sample number	A_b 210 min [%]	A_b 270 min [%]	A_b 320 min [%]	A_b 1440 min [%]	A_b 2880 min [%]	A_b 4320 min [%]	A_b 8640 min [%]	A_b 10080 min [%]	A_b 11520 min [%]	A_b average [%]
9085	8.14	8.18	8.21	8.25	8.42	8.66	8.73	5.60	8.79	8.46
9086	9.23	9.24	9.24	9.38	9.57	9.72	9.82	6.02	9.96	9.56
9087	8.85	8.86	8.87	9.03	9.24	9.46	9.54	2.41	9.65	9.24
9088	10.62	10.62	10.64	10.79	10.99	11.31	11.42	2.65	11.50	11.04
9089	5.86	5.88	5.90	6.01	6.19	6.40	6.49	2.32	6.53	6.2
9090	9.47	9.46	9.47	9.66	9.84	10.13	10.15	2.75	10.27	9.86
9091	10.12	10.12	10.14	10.43	10.56	10.89	10.98	4.12	11.10	10.6
9092	10.87	10.90	10.92	11.13	11.35	11.59	11.65	2.65	11.82	11.34
9093	9.21	9.23	9.25	9.39	9.55	9.78	9.82	2.61	9.96	9.57
9094	9.35	9.37	9.34	9.44	9.65	9.92	9.98	3.88	10.13	9.7
Average	9.17	9.19	9.20	9.35	9.54	9.79	9.86	9.95	9.97	9.56

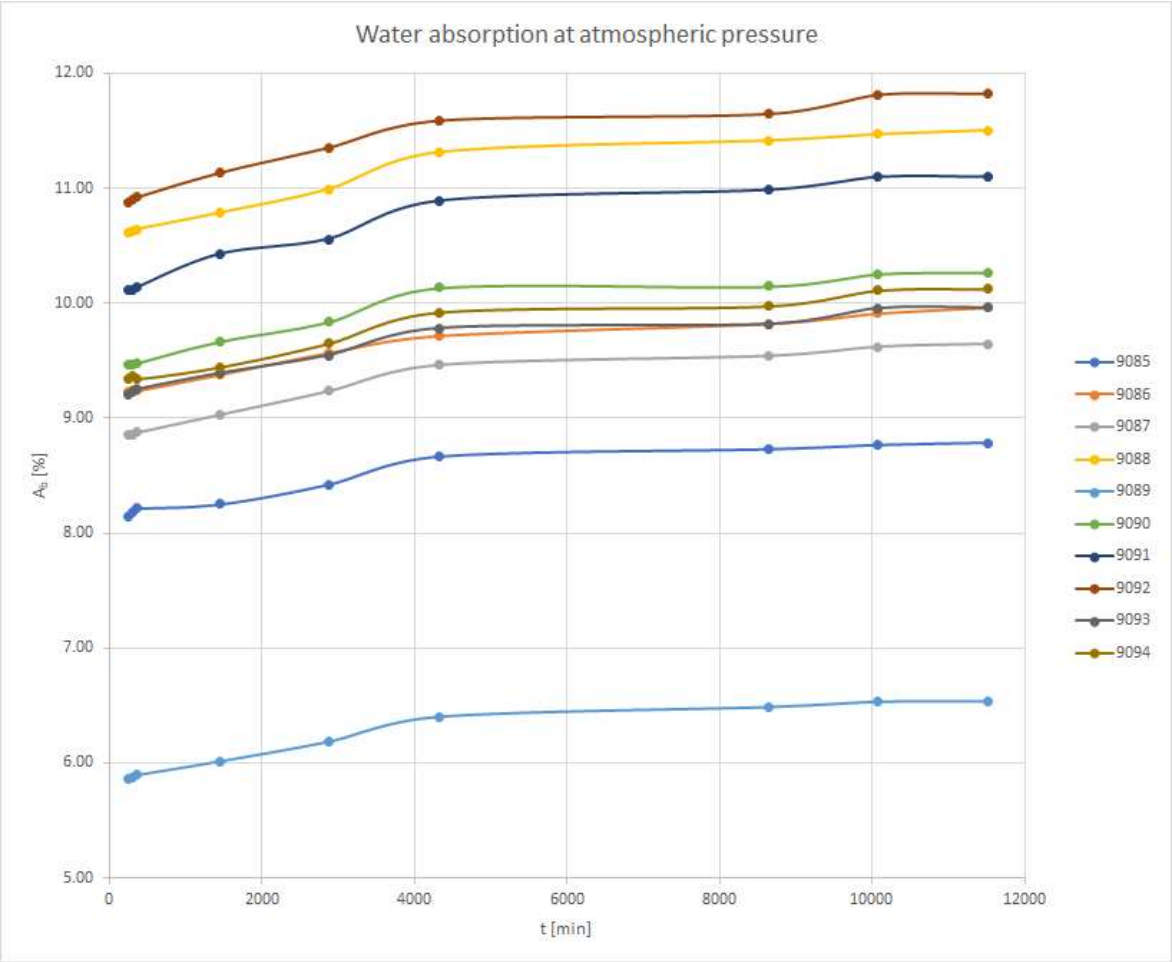

Figure 5-6. Graphical presentation of the water absorption of the second set of samples

5.5. The results of determining the apparent density, total and open porosity of the samples

Both sets of samples were tested under the norm HRN EN 1936: „Natural stone test methods – Determination of real density and apparent density, and of total and open porosity (EN 1936:1999)“. Open porosity was calculated using two different equations: 3-6 (p_{o1}) and 3-9 (p_{o2}). Apparent density was calculated using the equation 3-5 (table 5-10. and table 5-12.). Total porosity was calculated using the equation 3-10. Also, the apparent volume can be calculated using the dimensions of the samples (V_{b1}) or by the equation 3-8 (V_{b2}). The volume of the open pores was calculated using the equation 3-7 (table 5-11. and table 5-13.).

Table 5-10. Calculating the open porosity, apparent density, and real density of the first set of samples

Sample number	m_d [g]	m_s [g]	m_h[g]	p_{o1}[%]	ρ_b [g/cm^3]	ρ_r [g/cm^3]
8962	254.45	268.93	141.57	11.37	1.99	2.45
8963	247.4	262.09	137.71	11.81	1.98	2.47
8964	268.3	274.97	148.07	5.26	2.11	2.48
8965	267.63	275.05	147.28	5.81	2.09	2.44
8966	276.1	282.88	156.1	5.35	2.17	2.51
8967	265.71	273.49	147.83	6.19	2.11	2.53
8968	253.2	263.59	139.1	8.35	2.03	2.42
8969	274.96	282.64	154.78	6.01	2.14	2.54
8970	259.65	266.56	143.47	5.61	2.10	2.33
8971	264.39	274.8	146.02	8.08	2.05	2.49

Table 5-11. Calculating the total porosity, apparent volume, open volume, and open porosity of the first set of samples

Sample number	p [%]	V_{b1} [cm^3]	V_{b2} [cm^3]	V_o [cm^3]	p_{o2}[%]
8962	18.68	129.47	127.84	14.53	11.37
8963	19.87	125.96	124.85	14.75	11.81
8964	15.15	125.96	127.38	6.70	5.26
8965	14.54	128.25	128.25	7.45	5.81
8966	13.47	124.76	127.26	6.81	5.35
8967	16.76	125.96	126.14	7.81	6.19
8968	16.20	125.96	124.96	10.43	8.35
8969	15.49	123.55	128.34	7.71	6.01
8970	9.72	125.97	123.56	6.94	5.61
8971	17.75	125.89	129.27	10.45	8.08

Table 5-12. Calculating the open porosity, apparent density, and real density of the second set of samples

Sample number	m_d [g]	m_s [g]	m_h[g]	p_{o1}[%]	ρ_b [g/cm^3]	ρ_r [g/cm^3]
9085	248.94	270.81	148.54	17.89	2.03	2.44
9086	245.67	270.14	143.43	19.31	1.93	2.35
9087	251.29	275.53	147.63	18.95	1.96	2.41
9088	236.16	263.33	138.14	21.70	1.88	2.42
9089	261.21	278.28	154.68	13.81	2.10	2.50
9090	237.60	262.00	139.47	19.91	1.93	2.45
9091	241.71	268.53	140.67	20.98	1.88	2.35
9092	240.87	269.34	140.58	22.11	1.86	2.47
9093	252.52	277.67	149.85	19.68	1.97	2.49
9094	254.32	280.07	150.47	19.87	1.95	2.46

Table 5-13. Calculating the apparent volume, open volume, and open porosity of the second set of samples

Sample number	p [%]	V_{b1} [cm^3]	V_{b2} [cm^3]	V_o [cm^3]	p_{o2}[%]
9085	16.74	125.05	122.78	21.96	17.89
9086	17.81	123.67	127.24	24.57	19.31
9087	18.82	123.67	128.44	24.34	18.95
9088	22.32	125.05	125.72	27.28	21.70
9089	15.96	124.36	124.12	17.14	13.81
9090	21.20	127.14	123.04	24.50	19.91
9091	19.97	125.74	128.40	26.93	20.98
9092	24.66	126.44	129.30	28.59	22.11
9093	20.86	130.67	128.36	25.26	19.68
9094	20.52	123.67	130.14	25.86	19.87

Regarding the first set of samples (table 5-10.) open porosity ranged from 5.26% up to 11.81%. The total porosity was greater and varied from 9.72% to 19.87 %. Regarding the second set of samples, open porosity ranged from 13.81% up to 22.11%. The total porosity was supposed to be greater and varied from 15.96% to 24.66%, but in the samples 9085, 9086, 9087 and 9091 was slightly smaller, probably due to an error in measuring. The second set of samples also had a greater water absorption then the first set of samples.

In both types of rock samples, there seems to be a strong link between open porosity and water absorption. This is shown by a R^2 values (Coefficient of determination) being close to 1. R-squared is one of the most used measures for linear regression. It uses a scale ranging from 0 to 1 with which it shows how well the independent variables in a model explain the variability in the outcome variable. The value R^2= 0 shows that the regression model does not explain any of the variation in the outcome variable, while R^2=1 indicates that the model explains all the variation in the outcome variable (Scheidel, 2020). That means that in both cases with the increase in open porosity, the water absorption increases proportionally (figure 5-7. and figure 5-8.). For the first set of samples, R^2 was 0.9995 and for the second set, R^2 was 0.9924 which means that in both cases, there was a strong relationship between water absorption at atmospheric pressure and open porosity.

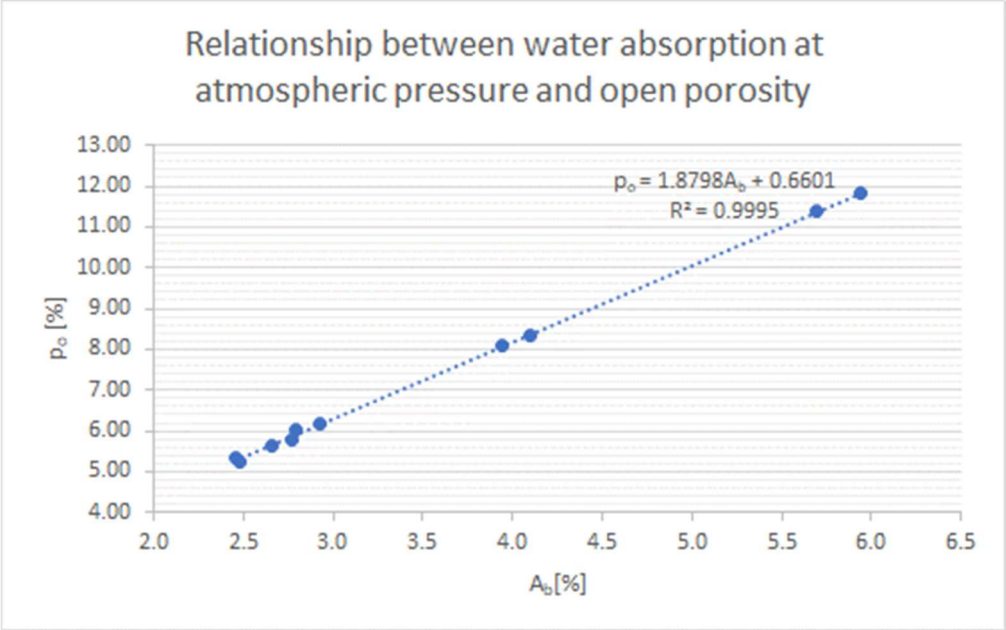

Figure 5-7. The relationship between the water absorption at atmospheric pressure and open porosity for the first set of samples

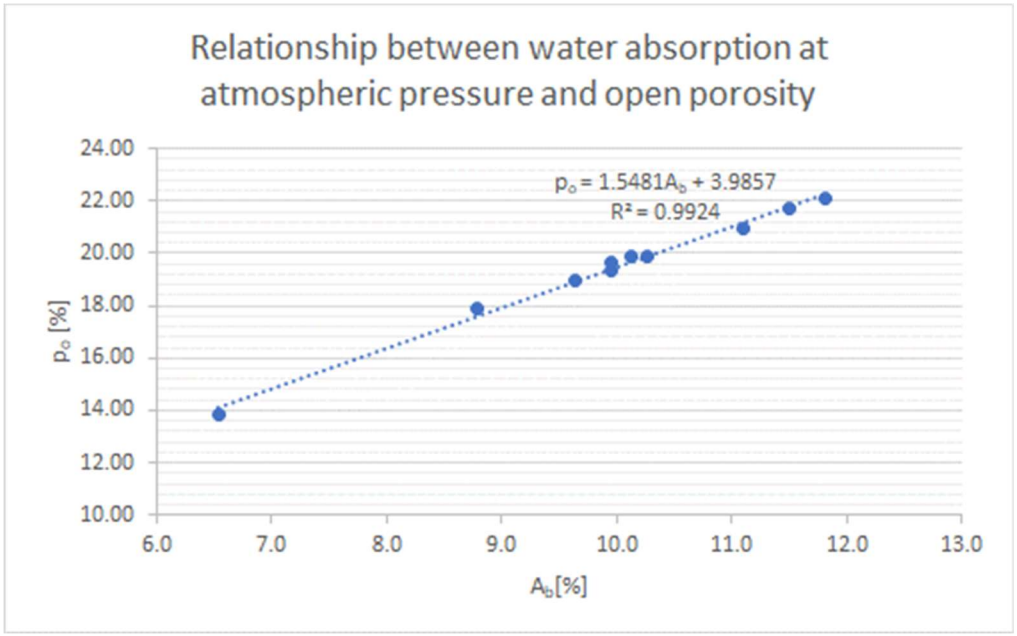

Figure 5-8. The relationship between the water absorption atmospheric pressure and open porosity for the second set of samples

6. DISCUSSION

The results of the stone composition and physical properties of the stone impact the decision if this type of limestone were to be used as a building stone. It also gives an insight into the types of limestone that could be used to replace lithothamnium limestone and/or sandstone in the future restoration works. The composition of only the lithothamnium limestone specimens (8962-8971) was determined with the most abundant minerals being calcite, dolomite and quartz.

6.1. The real density of the samples

Regarding the real density of the samples, the lowest value was of the 2327.81 kg/m^3 (sample 8970) and the highest value was 2535.10 kg/m^3 (sample 8969) with the difference between the values being 207.28 kg/m^3. This gives a narrow range of values for the real density between the samples. This is within the expected range for limestone (2300-2700 kg/m^3) (Alden, 2020). The mean value of the real density of all the samples was 2449.60 kg/m^3. In test done in 1995 on three limestone core samples from the Zagreb Catedral's tympanum, the real density was 2.7 g/cm^3 (Crnković, 1995) making the average value of real density calculated in this thesis smaller. Real density values are about the same as when compared with those of other building stones, e.g., the real densities of calcareous sandstone are 2.47 (g/cm^3) (Pavía, 1994 & Pavía, 2005).

Following the norm ASTM C568/C568M-15 „Standard Specification for Limestone Dimension Stone" all the samples fall within the Class II of the limestone dimension stone, being of medium density (table 6-1.). This means that, considering only the real density of the samples and following the norm ASTM C-568, both sets of samples could be used in construction.

Table 6-1. Standard specification for limestone dimension stone as in ASTM C568/C568M-15 „Standard Specification for Limestone Dimension Stone" (Beall, 1989 & Khayyun, 2019)

Classification Number	Consistency degree	Water absorption	Density (kg/m^3)
Class I	Low density	7.5-12%	1760-2160
Class II	Medium density	3-7.5%	2160-2560
Class III	High density	<3	>2560

6.2. The apparent density, open and total porosity of the samples

Regarding the apparent density, the values range from 1862.88 kg/m^3 (sample 9092) to 2169.57 kg/m^3 (sample 8966), with the difference being 306.70 kg/m^3. This is in accordance with the testing done in 1995 on 12 limestone samples from the Zagreb Cathedral in which the apparent density ranged from 1.878 g/cm^3 to 2.123 cm/g^3 (Crnković, 1995)

The mean value of the apparent density for all 20 samples were 2012.60 kg/m^3. The apparent density values are high when compared with those of other building stones, e.g., typical apparent densities of calcareous sandstone are 1.57 g/cm^3 (Pavía, 1994 & Pavía, 2005). The apparent density is also higher than other Miocene limestones such as sandy limestones from Eniwetok Atoll, Marshall Island, which have a dry apparent density of 1.21 g/cm^3, but also has a lesser apparent density then the Miocene limestone from Canton Schaffilausen, Switzerland that have the apparent density of 2.24 g/cm^3 when dry and 2.42 g/cm^3 when saturated with water (Manger, 1963).

Open porosity of the samples ranged from 5.26% (sample 8964) to 22.12% (sample 9092), with the difference between those values being 16.85%. The mean value of all the samples was 13.40%. The average open porosity was within the normal range for limestones (table 6-2.)

Table 6-2. Average values of the real density and open porosity of various limestones (Vandevoorde et al., 2009)

Material	Symbol	Real density (kg/m^3)	Open porosity (%)
Limestone			
Massangis Roche Claire	MC	2427 ± 5	10.7 ± 0.2
Massangis Roche Jaune	MJ	2400 ± 120	10.5 ± 0.9
Senoville	S	2388 ± 7	10.6 ± 0.2
Valanges	V	2300 ± 100	14 ± 2
Magny Doré	M	2290 ± 20	15.6 ± 0.8
Tercé	T	2060 ± 75	24 ± 5
Estaillades	E	1920 ± 20	29.3 ± 0.6

Total porosity of samples varied between 9.72% (sample 8970) and 24.66% (sample 9092), giving the difference of 14.93%. The mean value of all the samples were 17.82%. This value was slightly smaller when compared to another Miocene limestone from Canton Schaffilausen, Switzerland that has the average value of total porosity 18.3% (Manger, 1963). The total porosity is within the normal range when compared with other sedimentary rocks such us calcareous sandstone, which usually ranges from 12 to 24%, and certain limestones which can reach up to 34% pore volume (Pavía, 1994 & Pavía, 2005). Porosity as one of the physical properties of rocks that can control the other parameter such as bulk density which was inversely proportional with porosity (Awadh, 2015).

The values of porosity calculated in 1995 form tests on 12 limestone core samples from the Zagreb Catedral's tympanum ranged from 21.37% to 31.15% (Crnković, 1995). The author did not specify if in that study the open or total porosity was calculated.

This values of the open porosity in 4 samples (9085, 9086, 9087 and 9091) are bigger than the values of their total porosity. Since these samples have high values of water absorption, the values of the open and total porosity are closer to each other, giving the possibility of open porosity being larger than the total porosity due the values being more sensitive to showing an opposite result than what is expected. This might have happened due to mistakes made during the measuring process, probably when the weighing of the samples. Also, in the paper written by Manger (1963) open porosity was too sometimes slightly bigger than the total porosity.

Porous stone should not be used as building stone. It weathers aways more easily because rainwater can enter the pour and reacts with stone and crumbles it (Balasubramanian, 2017). Another problem is that water might freeze and turn into ice, further destroying the rock.

6.3. The water absorption at atmospheric pressure of the samples

The final value of water absorption at atmospheric pressure of the samples ranged from 2.46% (sample 8966) to 11.82% (sample 9092) with the difference being 9.36 %. The mean value was 6.77%.

After the first 24 hours of being submerged, the water absorption at atmospheric pressure ranged from 2.27% (sample 8966) to 11.13% (sample 9092) with the difference between them being 8.86%. The mean value is 6.39%. The values of water absorption calculated in 1995 from the test on 12 limestone core samples from the Zagreb Catedral's tympanum ranged from 2.10% to 10.92% (Crnković, 1995) which is in accordance with the values calculated in this thesis.

According to Balasubramanian (2017), the maximum limit of water absorption after being submerged for 24 hours for limestone should not exceed 10% if it were to be used as building stone (table 6-3.). Some of the samples did exceed this maximum limit. Also, according to the table 6-1., the final water absorption at atmospheric pressure was within all three categories of the rock, which is not ideal.

Table 6-3. Permissible limits of water absorption for some the commonly used building stones (Balasubramanian, 2017)

Type of Stone	Maximum limit of Water Absorption (%)
Sandstone	10
Limestone	10
Granite	1
Shale	10
Slate	1
Quartzite	3

This means that this limestone has a high-water absorption at atmospheric pressure. The water absorption of porous stone material is an indication of the degree of deterioration and its sensitivity to future deterioration (Vandevoorde et al., 2009). Therefore, it would be best if the value of water absorption at atmospheric pressure was lower if this type of stone were to be used in building again.

7. CONCLUSION

In this study, 20 samples taken from large pieces of rock that had fallen from the Zagreb Cathedral during the 2020 earthquake were tested. They were of Miocene Lithothamnium limestone and sandstone mined from the Medvednica Mountain near Zagreb.

The results of the X-Ray Diffraction showed that the samples consisted mostly of calcite and quartz, with the possibility of some dolomite, plagioclase, K-feldspar, mica, kaolinite and/or chlorite.

The results of the real density analysis showed that it ranged from 2327.81 kg/m^3 to 2535.10 kg/m^3 with the mean value being 2449.60 kg/m^3. This makes this limestone a medium density limestone and places it's real density within the expected range of limestones.

The results of the apparent density range from 1862.88 kg/m3 to 2169.57 kg/m^3, with the difference being 306.70 kg/m^3 with mean value being 2012.60 kg/m3. This makes it comparable to other Miocene limestones. According to Pavía (1994) & Pavía (2005), this puts this limestone with the range of apparent density that is suitable for construction.

The results of the open porosity ranged from 5.26% to 22.12% with the mean value of being 13.40%. This puts it within the normal range of limestones.

The results of the total porosity of samples varied between 9.72% and 24.66% with the mean value of all the samples being 17.82%. This puts it within the normal range of limestones.

The results of water absorption at atmospheric pressure varied between 2.46% and 11.82% with the mean value being 6.77%. This was a range and according to the ASTM C568/C568M-15 „Standard Specification for Limestone Dimension Stone" samples from this study fall within all 3 classes of limestone. According to Balasubramanian (2017), the maximum limit of water absorption after being submerged for 24 hours for limestone should not exceed 10% or it is not suitable as building stone. Some of the tested samples did exceed this limit while others were below them.

These 20 tested samples all fell within the expected range for lithothamnium limestone. If the same type of rock were to be used in building again, it could face problems from weathering due being porous hence having high water absorption at atmospheric pressure which damages the rock over time.

In the future, the mineral composition of sandstone specimens should be done to ensure that the stone can be used for future building projects. Also, the other physical and mechanical properties of lithothamnium limestone and sandstone should be tested since they too play a vital role in the selection of stone as a building material.

8. LITERATURE

Online materials

Alde, A. 2020. *Densities of Common Rocks and Minerals*. ThoughtCo.. URL: https://www.thoughtco.com/densities-of-common-rocks-and-minerals-1439119 (12.2.2022.)

Awadh, S.M. 2015. *Assessment of sandstone in western desert of Iraq as anti-acidic and alkalis benches*. ResearchGate. URL: https://www.researchgate.net/figure/Physical-and-mechanical-properties-of-sandstone-in-Rutbah-Formation_tbl2_305279691 (3.3.2022.)

Balasubramanian, A. 2017. *PROPERTIES OF BUILDING STONES*. University of Mysore. ReseachGate. URL: https://www.researchgate.net/publication/319306760_PROPERTIES_OF_BUILDING_STONES (4.5.2022.)

Beall, C. 1989. *Selecting the right stone*. URL: https://www.concreteconstruction.net/_view-object?id=00000154-22dd-db06-a1fe-73dde10a0000 (2.5.2022.)

Chemistry Library$_a$. 2020. *Bragg's Law*, LibreTexts. URL: https://chem.libretexts.org/ (22.3.2022.)

Chemistry Library$_b$ (2020): *Powder X-ray Diffraction*, LibreTexts. URL: https://chem.libretexts.org/ (22.3.2022.)

Deutscher Naturwerkstein-Verband e.V..2016. *Europäisches Logo für Naturstein*. URL: https://www.natursteinverband.de/naturstein/steinzeichen.html (15.3.2022.)

Dutrow, B. L., Clark, C. M. 2022. *X-ray Powder Diffraction (XRD)*. The Science Education Resource Center. URL: https://serc.carleton.edu/research_education/geochemsheets/techniques/XRD.html#:~:text=A%20peak%20in%20intensity%20occurs%20when%20the%20mineral%20contains%20lattice,side%20of%20K%CE%B11 (15.3.2022.)

Epiroc. 2020. *Dimension stone industry*. URL: https://www.epiroc.com/en-ro/applications/construction/quarrying-and-surface-construction/dimension-stone-industry (21.4.2022.)

Informativna katolička agencija. 2020. *U potresu nastala nova oštećenja na zagrebačkoj katedrali.* URL: https://ika.hkm.hr/novosti/u-potresu-nastala-nova-ostecenja-na-zagrebackoj-katedrali/ (16.6.2022.)

Khayyun, T. 2019. *Comparison of the experimental results with the Langmuir and Freundlich models for copper removal on limestone adsorbent*. ReseachGate. URL: https://www.researchgate.net/ (3.5.2022.)

Klein, C. 2021. *rock. Definition, Characteristics, Formation, Cycle, Classification, Types, & Facts.* Britannica. URL: https://www.britannica.com/science/rock-geology

Malik, R. 2018. *Building Stones: Meaning and Properties.Geography notes.* URL: https://www.geographynotes.com/geology-2/building-stones/building-stones-meaning-and-properties-geology/5924 (12.5.2022.)

Manger, E. G. 1963. *Porosity and Bulk Density of Sedimentary Rocks*, GEOLOGICAL SURVEY BULLETIN 1144-E. URL: https://pubs.usgs.gov/bul/1144e/report.pdf (16.4.2022.)

Ministarstvo obrane Republike Hrvatske. 2020. *Povijesni pothvat Hrvatske vojske uklanjanja tornja zagrebačke katedrale.* URL: https://www.morh.hr/povijesni-pothvat-hrvatske-vojske-uklanjanja-tornja-zagrebacke-katedrale/ (2.3.2022.)

Narod.hr. 2021. *Počinje zahtjevna konstrukcijska obnova zagrebačke katedrale*. URL: https://narod.hr/kultura/pocinje-zahtjevna-konstrukcijska-obnova-zagrebacke-katedrale (23.4.2022.)

Pavía, S. 2005. *Design of quality, durable mortar for the conservation of historic masonry fabrics. Trinity College Dublin*. ResearchGate, URL: https://www.researchgate.net/publication/277231471_Design_of_quality_durable_mortar_for_the_conservation_of_historic_masonry_fabrics (12.3.2022.)

Perkins, D. 2020. *12. X-ray Diffraction and Mineral Analysis, Mineralogy, University of North Dakota*, 1-30 URL: https://opengeology.org/Mineralogy/12-x-ray-diffraction-and-mineral-analysis/ (22.4.2022.)

Prirodoslovno-matematički fakultet u Zagrebu. 2022. *DVIJE GODINE OD ZAGREBAČKOG POTRESA*. Geofizički odsjek. URL: https://www.pmf.unizg.hr/geof/seizmoloska_sluzba/o_zagrebackom_potresu_2020/druga_godisnjica_zagrebackog_potresa (14.3.2022.)

Scheidel, C. 2020. *What is R-squared?, Methods Consultants*. URL: https://tutorials.methodsconsultants.com/posts/what-is-r-squared-understanding-the-coefficient-of-determination/ (12.3.2022.)

Speakman, S. A. 2014. *Basics of X-Ray Powder Diffraction*. URL: http://prism.mit.edu/xray/oldsite/Basics%20of%20X-Ray%20Powder%20Diffraction.pdf (12.3.2022.)

Vandevoorde, D., Pamplona, M., Schalm, S.,Vanhellemont, Y., Cnudde, V., Verhaeven, E. 2009. *Contact sponge method: Performance of a promising tool for measuring the initial water absorption*. ResearchGate. Journal of Cultural Heritage 10 (2009) 41-47. URL: https://www.researchgate.net/publication/233382377_Contact_sponge_method_Performance_of_a_promising_tool_for_measuring_the_initial_water_absorption (14.2.2022.)

Winkler, E.M. 1997. *Physical Properties of Stone. In: Stone in Architecture*. Springer, Berlin, Heidelberg. URL: https://doi.org/10.1007/978-3-662-10070-7_2 (12.3.2022.)

Books

Crnković, B. 1992. *Restauratorski radovi na Zagrebačkoj* katedrali. Klesarstvo i graditeljstvo, str. 1-2, 3, 19-21.

Crnković, B. 1994. *Obnova zagrebačke katedrale.* Klesarstvo i graditeljstvo, V, str. 1-2, 1994., 32-39.

Crnković, B. 1995. *Zagrebačka katedrala Istraživački radovi na timpanonu*. Klesarstvo i graditeljstvo, VI., str. 1-2, 21-28.

Fio Firi, K., Maričić, A. 2020. *Usage of Natural Stones in the City of Zagreb (Croatia) and its Geotouristical Aspect.* Geoheritage, 12:62, str. 1 – 18.

Pavía, S. 1994. *Material de construcción antiguo de Logroño y La Rioja Alta: petrografía, propiedades físicas geología y alteración*. Instituto de Estudios Riojanos, str. 247

Magazines

Crnković, B. 1996. *Kamen Zagrebačke prvostolnice*. Godišnjak zaštite spomenike kulture Hrvatske, str. 27-34.

Crnković, B., Poggi, F. 1995. *Travertine the restoration stone for the Zagreb Cathedral*. Rudarsko-geološko-naftni zbornik, str. 7, 77–85.

Dolley, T.P. 2018. *2018 Minerals Yearbook [ADVANCE RELEASE], Stone, Dimension*. United States Geological Survey, str. 72.1

Flohr, M.J.K. 1997. *X-Ray Powder Diffraction, United States Geological Survey*. URL: https://pubs.usgs.gov/info/diffraction/xrd.pdf (14.3.2022.)

Manuals

Eijkelkamp Agrisearch Equipment (2012): 08.53 calcimeter. URL: https://www.royaleijkelkamp.com/media/qfgn1ma0/manual-calcimeter.pdf

Master's thesis'

Salinger, T. 2020. *Zagrebačka katedrala - obnova kroz povijest (s naglaskom na razdoblju između dva potresa)*. University of Rijeka, Faculty of Humanities and Social Sciences, str. 2-5, 21, 24